© 2014. Published by The Company of Biologists Ltd | Journal of Cell Science (2014) 127, 1751–1764 doi:10.1242/jcs.138230

RESEARCH ARTICLE

Mutations in Cx30 that are linked to skin disease and non-syndromic hearing loss exhibit several distinct cellular pathologies

Amy C. Berger[1,*], John J. Kelly[2,*], Patrick Lajoie[2], Qing Shao[2] and Dale W. Laird[1,2,‡]

ABSTRACT

Connexin 30 (Cx30), a member of the large gap-junction protein family, plays a role in the homeostasis of the epidermis and inner ear through gap junctional intercellular communication (GJIC). Here, we investigate the underlying mechanisms of four autosomal dominant Cx30 gene mutations that are linked to hearing loss and/or various skin diseases. First, the T5M mutant linked to non-syndromic hearing loss formed functional gap junction channels and hemichannels, similar to wild-type Cx30. The loss-of-function V37E mutant associated with Clouston syndrome or keratitis-ichthyosis-deafness syndrome was retained in the endoplasmic reticulum and significantly induced apoptosis. The G59R mutant linked to the Vohwinkel and Bart-Pumphrey syndromes was retained primarily in the Golgi apparatus and exhibited loss of gap junction channel and hemichannel function but did not cause cell death. Lastly, the A88V mutant, which is linked to the development of Clouston syndrome, also significantly induced apoptosis but through an endoplasmic-reticulum-independent mechanism. Collectively, we discovered that four unique Cx30 mutants might cause disease through different mechanisms that also likely include their selective trans-dominant effects on coexpressed connexins, highlighting the overall complexity of connexin-linked diseases and the importance of GJIC in disease prevention.

KEY WORDS: Connexin, Gap junction, Hemichannel, Hearing loss, Skin disease, Mutation, Vohwinkel syndrome, Bart-Pumphrey syndrome, Clouston syndrome, Keratitis-ichthyosis-deafness syndrome

INTRODUCTION

Gap junctions are clusters of specialized intercellular channels that regulate the direct exchange of ions and various hydrophilic cellular metabolites that are smaller than 1000 Da, a process known as gap junctional intercellular communication (GJIC) (Alexander and Goldberg, 2003). Two inter-docked connexons (hemichannels), one from each of two apposing cells, form a functional gap junction channel. Each connexon is composed of six oligomerized connexin (Cx) subunits, and, to date, the connexin family consists of 21 members in human (Söhl and Willecke, 2003; Söhl and Willecke, 2004). Interestingly, the primary function of gap junction channels is to facilitate intercellular communication; however, hemichannels have also been reported to exist and function at the cell surface in an undocked state, permitting the transfer of molecules between extracellular and intracellular environments (Anselmi et al., 2008; Burra and Jiang, 2011; Tong et al., 2007). Hemichannels that are formed from single or multiple types of connexins are termed homomeric and heteromeric, respectively, and gap junction channels are characterized as homotypic or heterotypic according to whether their channels are composed of the same or different connexions, respectively (Burra and Jiang, 2011). The composition of the channel depends on the connexin expression profile of each cell and tissue type, as well as the natural compatibility of the connexins in order for them to intermix (Beyer et al., 2013; Burra and Jiang, 2011; Laird, 2006).

Connexins are highly expressed in virtually all tissues in the human body, and GJIC plays an essential role in the regulation of cellular and physiological processes including proliferation, differentiation, apoptosis, growth and development (Alexander and Goldberg, 2003; Choudhry et al., 1997; Decrock et al., 2009; Kumar and Gilula, 1996; McLachlan et al., 2007). In the inner ear and the skin, proper connexin expression and function directly relate to the maintenance of cochlear homeostasis and epidermal differentiation, respectively (Langlois et al., 2007; Wangemann, 2006; Zhao et al., 2006). In the cochlea, Cx26, Cx29, Cx30, Cx31 and Cx43, found in the epithelial and connective tissue gap junction networks, play a crucial role in sound transduction. Cx26, and possibly other connexins, are thought to be involved in the recycling of K^+ through the supporting cells back to the endolymphatic space, for potential re-entry into sensory cells when activated by an acoustic stimulus (Kikuchi et al., 2000; Nickel and Forge, 2008). Interestingly, at least seven connexins, including Cx26, Cx30 and Cx43, are temporally and spatially expressed at the protein level in the human epidermis with overlapping distribution in the various non-cornified epidermal strata (Di et al., 2001; Kretz et al., 2004). GJIC plays an important role in epidermal differentiation: however, it is also critical to the wound healing process (Churko and Laird, 2013; Langlois et al., 2007). Here, we focus on Cx30, which, in human, is predominantly expressed in the inner ear and epidermis (Di et al., 2001; Nickel and Forge, 2008).

Connexin mutations have been linked to a number of different diseases ranging from developmental disorders to congenital cataracts (Laird, 2006). Mutations in the genes encoding Cx26, Cx30, Cx30.3 and Cx31, in particular, have been linked predominantly to hearing loss and various skin diseases (Di et al., 2001). Importantly, mutations in Cx30 and Cx26, the most predominant connexins in the inner ear (Hoang Dinh et al., 2009), are the leading cause of nearly half of the cases of inherited prelingual non-syndromic hearing loss (Bitner-Glindzicz, 2002; Chang et al., 2009; Schutz et al., 2010; Wang et al., 2011). In particular, seven distinct single amino acid substitutions in

[1]Department of Physiology and Pharmacology, University of Western Ontario, London, ON N6A 5C1, Canada. [2]Department of Anatomy and Cell Biology, University of Western Ontario, London, ON N6A 5C1, Canada.
*These authors contributed equally to this work

‡Author for correspondence (Dale.Laird@schulich.uwo.ca)

Received 9 July 2013; Accepted 22 January 2014

Journal of Cell Science (2014) 127, 1751–1764 doi:10.1242/jcs.138230

the first half of the coding sequence of Cx30 are responsible for hearing loss and/or skin disease. The T5M (threonine to methionine at position 5) and A40V (alanine to valine at position 40) mutations have been linked to non-syndromic hearing loss because no other tissues or organs where Cx30 is expressed were affected (Grifa et al., 1999; Wang et al., 2011). Interestingly, hidrotic ectodermal dysplasia, commonly known as Clouston syndrome, is a skin disease distinctly linked to G11R (glycine to arginine at position 11) (Chen et al., 2010; Common et al., 2002; Zhang et al., 2003), V37E (valine to glutamic acid at position 37) (Common et al., 2002; Jan et al., 2004; Smith et al., 2002), D50N (aspartic acid to asparagine at position 50) (Baris et al., 2008) and A88V (alanine to valine at position 88) (Common et al., 2002; Essenfelder et al., 2004) Cx30 mutations. This rare disease has a founder effect within the French–Canadian population and is characterized by palmoplantar hyperkeratosis (PPK), nail dystrophies and partial to complete alopecia (Kibar et al., 2000; Zhang et al., 2003). In some patients, other symptoms – such as ocular and craniofacial abnormalities, hearing loss, and abnormal sweating and cardiac findings – have been reported (Christianson and Fourie, 1996; Fraser and Der Kaloustian, 2001; Lamartine et al., 2000). Interestingly, one patient harboring a V37E Cx30 mutation was diagnosed with keratitis-ichthyosis-deafness (KID) syndrome, which is commonly associated with Cx26 mutations. This patient experienced Clouston-syndrome-like symptoms but also hearing impairment and vascularising keratitis (Jan et al., 2004). Finally, a G59R mutation results in the development of classical Vohwinkel syndrome and Bart-Pumphrey syndrome (Nemoto-Hasebe et al., 2009), which are also diseases that are most commonly caused by mutations in Cx26 (Bakirtzis et al., 2003; Jan et al., 2004; Richard et al., 2004). Both syndromes result in PPK and sensorineural hearing loss, however, Bart-Pumphrey syndrome can be distinguished by the formation of knuckle pads, whereas patients with Vohwinkel syndrome develop constriction bands that cause spontaneous auto-amputation of the digits (pseudoainhum) (Bakirtzis et al., 2003; Richard et al., 2004).

Previously, studies on a few of the Cx30 disease-linked mutations have revealed reduced or abolished gap junction function, because a substantial amount of the mutant proteins are retained in subcellular compartments (Common et al., 2002; Essenfelder et al., 2004; Wang et al., 2011). Typically, most connexins follow the traditional secretory pathway of folding in the endoplasmic reticulum (ER), oligomerizing into connexons in either the ER or Golgi apparatus and then employing microtubules for efficient trafficking to the plasma membrane (Koval, 2006; Laird, 2006). Disruptions to any stage of this connexin transport process can have detrimental effects on cells and commonly results in connexin-linked disease (Laird, 2006).

Connexin mutations can lead to trafficking defects and their retention within the cell. In particular, the intracellular accumulation of Cx50 and Cx31 mutants causes cell death that is associated with the activation of ER-stress signaling pathways (Alapure et al., 2012; Tattersall et al., 2009). The aberrant accumulation of misfolded secretory proteins in the ER triggers a process known as the unfolded protein response (UPR) (Malhotra and Kaufman, 2007). Typically, quality control mechanisms involve chaperones in the ER that facilitate the re-folding of misfolded proteins for export out of the ER (Groenendyk and Michalak, 2005). The UPR involves the activation of three ER-membrane-bound sensors (PERK, IRE1 and ATF6), which work collectively to attenuate protein translation, increase the folding capacity of the ER through the upregulation of chaperone proteins, increase lipid synthesis and force misfolded proteins through an ER-associated degradation pathway in order to relieve ER stress and maintain cellular homeostasis (Malhotra and Kaufman, 2007). Failure of these processes to reduce ER stress results in the induction of apoptosis (Groenendyk and Michalak, 2005; Rasheva and Domingos, 2009).

Currently, it is poorly understood how Cx30 mutations manifest into syndromic and non-syndromic diseases involving the skin and cochlea. In the present study, we characterize four different Cx30 mutants, which are linked to non-syndromic hearing loss, Clouston syndrome, KID syndrome and Vohwinkel/Bart-Pumphrey syndromes to gain crucial insight into the mechanisms underlying these distinct disease manifestations. Our results indicate that the T5M mutant that is associated with non-syndromic hearing loss formed functional gap junction channels, whereas mutants that are linked to skin disease were primarily retained in intracellular compartments, reducing channel function. In addition, because we show here that mutants that are linked to Clouston syndrome induced cell death in keratinocytes, we investigate the potential mechanisms that mediate cell death. Surprisingly, the ER-localized V37E mutant did not substantially and consistently increase the expression of classical UPR markers, as would be predicted for misfolded proteins that accumulate in the ER. However, the V37E and A88V mutants activated a caspase-3 cleavage pathway to induce apoptosis. Finally, we demonstrate that the effects of mutations that are linked to skin disease are not rescued by coexpression with wild-type Cx30 or Cx26 in rat epidermal keratinocytes (REKs), and, in particular, that mutants associated with Clouston syndrome exhibit dominant-negative properties on these coexpressed connexins. Collectively, these studies demonstrate the complexity of the mechanisms that are involved in connexin-linked diseases, especially as one Cx30 mutant exhibits intercellular channel and hemichannel function but still causes disease.

RESULTS

Cx30 mutations linked to skin disease and non-syndromic hearing loss, and their differential ectopic expression and localization in REKs

Cx30 is a 261 amino acid gap junction protein that exhibits the topological structure of a typical connexin: four transmembrane domains, two extracellular loops, one intracellular loop and cytoplasm-exposed N- and C-termini (Fig. 1A). The location of four distinct mutations that cause skin disease and/or hearing loss are all located within the first half of the Cx30 protein (Fig. 1A).

Western blot analysis was used to determine the expression levels of green fluorescent protein (GFP)-tagged T5M, V37E, G59R and A88V mutants in REKs. Quantification of densitometry values revealed that V37E–GFP and A88V–GFP protein levels were ~35% and ~50% lower, respectively, compared with the relative expression of Cx30–GFP (**$P<0.01$) (Fig. 1B,C). By contrast, the mutants that are associated with non-syndromic hearing loss and Vohwinkel syndrome (T5M and G59R, respectively) exhibited expression levels similar to that of Cx30–GFP.

To compare the localization profiles of the mutant forms of Cx30, we examined GFP-tagged Cx30 mutants (Fig. 2A) and untagged Cx30 mutants (Fig. 2B,C) in REKs. Consistent with previous reports, the T5M mutant formed gap-junction-like plaques at the cell surface similar to wild-type Cx30, whereas

Journal of Cell Science (2014) 127, 1751–1764 doi:10.1242/jcs.138230

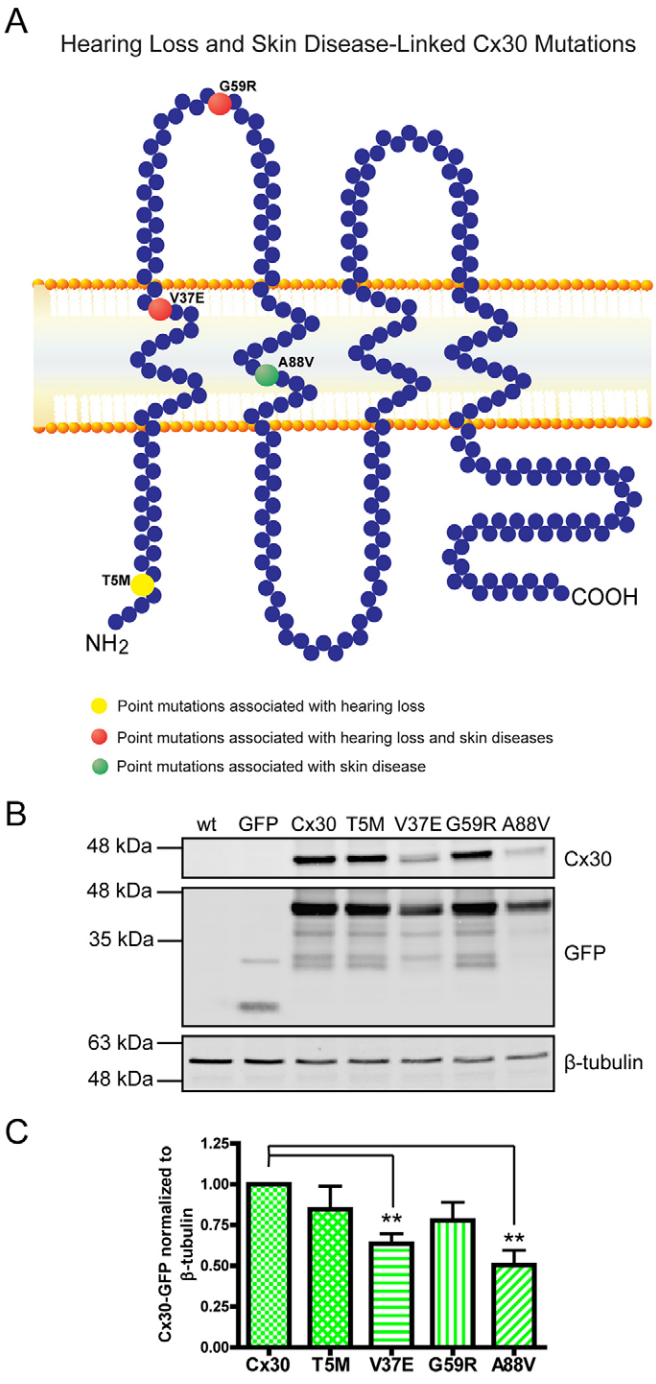

Fig. 1. Cx30 mutations linked to hearing loss and skin diseases, and their differential ectopic expression in REKs. (A) Cx30 depicting four mutations. The mutations are associated with hearing loss (yellow), hearing loss plus skin disease (orange) and skin disease (green). (B) Western blot analysis was used to detect the levels of GFP-tagged Cx30 and Cx30 mutants when ectopically expressed in REKs. The blots were probed with antibodies against Cx30, GFP or β-tubulin. wt, untransfected wild-type cells. (C) Western blotting for GFP revealed significantly lower levels of GFP-tagged V37E and A88V mutants compared with the levels of wild-type Cx30. Values represent the mean fold change±s.e.m., $^{**}P<0.01$, unpaired *t*-test, $n=3$.

the V37E and A88V mutants that are linked to Clouston syndrome appeared to remain in intracellular compartments (Common et al., 2002; Essenfelder et al., 2004) (Fig. 2A,B). Immunolabeling for the ER-resident protein disulfide isomerase (PDI) revealed that the V37E mutant, which is linked to the Clouston and KID syndromes, was retained in the ER (Fig. 2A). Cells expressing the A88V mutants appeared to be entering a cell death pathway because they exhibited small and fragmented nuclei; however, it remains unclear whether a substantial amount of this mutant resides in the ER because these cells lacked PDI staining. The novel Vohwinkel-syndrome-linked G59R mutant (Nemoto-Hasebe et al., 2009) also showed an intracellular localization profile (Fig. 2A,B), and immunolabeling for Golgi matrix protein 130 (GM130) revealed that the mutant was mainly localized in the Golgi apparatus (Fig. 2C). Interestingly, we never observed plaques that had formed from the V37E mutant at the interface between apposing cells; however, here, a population of the G59R and A88V mutants successfully trafficked to the cell surface to form gap-junction-like plaques (Fig. 2A,B, arrows). Wild-type Cx30 and the Cx30 mutants all exhibited similar localization patterns in cells, regardless of the presence or absence of the GFP tag (Fig. 2A–C).

The V37E and A88V Cx30 mutants affect localization of endogenous Cx43 in REKs and localization of ectopic Cx43 in HeLa cells

To determine whether the presence of the Cx30 mutants affected endogenous Cx43 localization, REKs were engineered to express Cx30–GFP or the equivalent GFP-tagged mutants. Upon expression of the T5M and G59R mutants, Cx43 frequently colocalized with Cx30 mutants at cell–cell interfaces, whereas Cx43-based gap junctions were observed less frequently between cells that expressed the V37E or A88V mutant (Fig. 3A). The total levels of the Cx43 proteins, however, remained unchanged (Fig. 3B,C). Total Cx43 levels showed only a small decrease in cells that expressed the T5M mutant compared to those that expressed wild-type Cx30 ($^{*}P<0.05$). In agreement with these findings, HeLa cells that had been engineered to coexpress Cx30 mutants with Cx43 that had been tagged with red fluorescent protein (Cx43–RFP) showed similar localization profiles (supplementary material Fig. S1). Both the wild-type Cx30 and the T5M mutant frequently colocalized in plaque-like structures, whereas cells expressing the V37E or A88V Cx30 mutants exhibited a lower amount of plaque formation and Cx43 was more evident in intracellular compartments. Cells that expressed the G59R mutant showed a reduced amount of plaque-like structures but Cx43 could still traffic to the cell surface (supplementary material Fig. S1).

The V37E and G59R Cx30 mutants are linked to skin disease and exhibit loss of gap junction function in HeLa cells

Since the T5M mutant and a proportion of the G59R mutant formed punctate gap-junction-like structures at the cell surface in REKs, we hypothesized that these mutants can form functional gap junctions. GJIC-deficient HeLa cells that expressed the Cx30 mutants were microinjected with Alexa Fluor 350 to assess whether any of the mutants restored GJIC. As expected, Cx30 gap junction channels readily facilitated dye transfer ($^{***}P<0.001$); however, untransfected cells (Untr) and cells that expressed free GFP showed no significant dye transfer to the surrounding cells (Fig. 4A,B). Interestingly, ~90% of cells that had been injected and expressed the T5M mutant exhibited dye transfer ($^{***}P<0.001$) (Fig. 4A,B), indicating that this mutant was functional. No dye transfer was observed in microinjected HeLa cells that expressed the V37E and G59R mutants

Journal of Cell Science (2014) 127, 1751–1764 doi:10.1242/jcs.138230

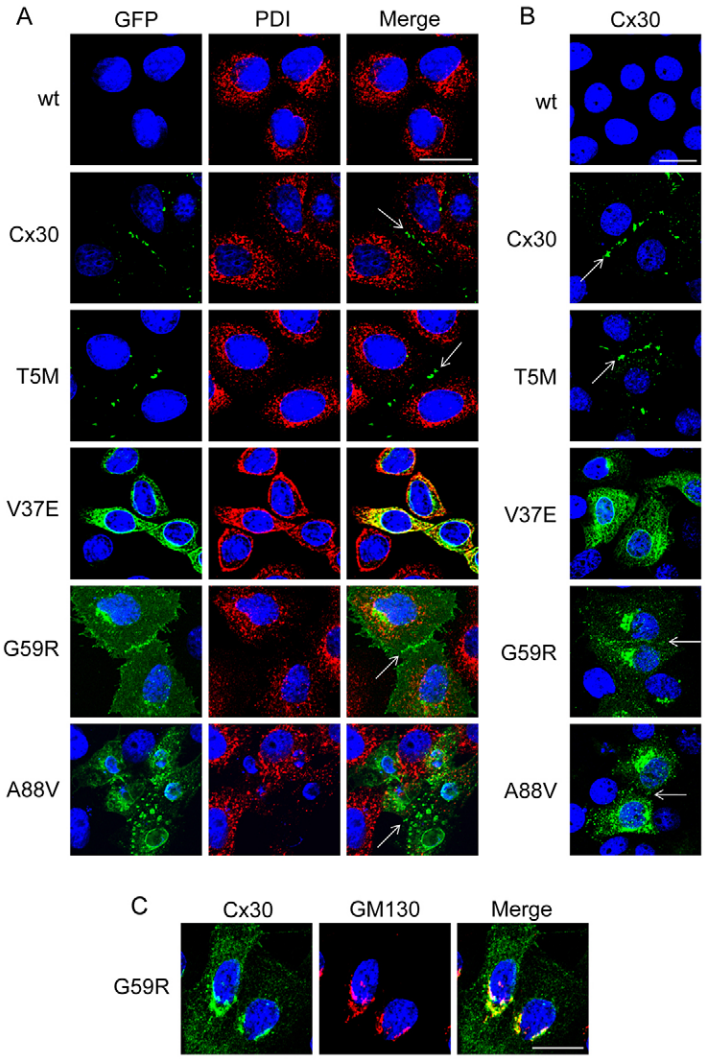

Fig. 2. Skin-disease-linked Cx30 mutants have impaired abilities to form gap junction plaques. (A) Untransfected REKs (wt) and REKs ectopically expressing GFP-tagged Cx30 or Cx30 mutants (green) were immunolabeled for protein disulfide isomerase (PDI) (red) to denote the ER. Nuclei were stained with Hoescht 33342 (blue). Cx30 and the T5M mutant proteins formed punctate gap-junction-like structures at the cell–cell interface, whereas the V37E mutant colocalized with PDI. The G59R and A88V mutants were, primarily, localized in intracellular compartments; however, a population of the mutants did reside at the cell surface (white arrows). PDI staining was absent in cells that expressed the A88V mutant, and GFP-positive cells without nuclei were discounted. (B) Immunolabeling REKs for Cx30 (green) revealed that cells expressing the untagged mutant proteins exhibited similar localization profiles to those that expressed GFP-tagged mutants. Similarly, some of the G59R and A88V mutant proteins localized to the cell surface (arrows). (C) REKs ectopically expressing the G59R mutant were double-labeled for Cx30 (green) and Golgi matrix protein 130 (GM130, red), which revealed that the G59R mutant colocalized with the Golgi apparatus. Colocalization is indicated in the merged images (yellow). Scale bars: 20 μm.

(Fig. 4A,B). A88V-expressing cells were not included in these functional studies because they could not be microinjected due to their porous cell membranes caused by cell death (see Fig. 5C).

The V37E and A88V Cx30 mutants reduce gap junctional intercellular communication in Cx43-positive REKs

Because the Cx30 mutants had the ability to affect Cx43 localization, we wanted to determine whether Cx30 mutants affected GJIC in Cx43-rich REKs. REKs that expressed the GFP-tagged mutants were microinjected with Alexa Fluor 350 in a region where the cell clusters were expressing GFP, and the incidence of dye transfer was recorded. Untransfected REKs exhibited 100% dye transfer, and no significant differences in dye transfer were observed in REKs expressing GFP, wild-type Cx30, or the T5M or G59R mutants (Fig. 4C,D). By contrast, cell pairs or clusters that expressed the V37E or A88V mutants exhibited significantly decreased Cx43-mediated dye transfer (**$P<0.01$) (Fig. 4C,D).

The V37E and G59R mutants do not form functional cell surface hemichannels

The ability of each Cx30 mutant to form functional hemichannels was investigated by observing the incidence of propidium iodide dye uptake in HeLa cells expressing the wild-type or mutant Cx30 proteins under normal extracellular solution (ECS) and Ca^{2+} and Mg^{2+} divalent-cation-free ECS (DCF-ECS) conditions, which induces hemichannel opening (Lai et al., 2006; Stout et al., 2002). Under ECS conditions, any putative Cx30, T5M, V37E or G59R mutant hemichannels remained closed and, as expected, no uptake of the dye was observed (Fig. 5A). Under DCF-ECS conditions, ~90% of isolated T5M-expressing cells exhibited uptake of the dye, closely resembling the ~95% incidence observed for cells that expressed Cx30, both of which were significantly higher than that observed under the control ECS conditions (***$P<0.001$) (Fig. 5A,B). By contrast, the cells expressing the V37E or G59R mutants did not exhibit any uptake of dye in DCF-ECS conditions. The loss of cell membrane integrity was evident in cells that expressed the A88V mutant because ~75% of the cells exhibited uptake of the hemichannel impermeable dye dextran–rhodamine (10-kDa molecular mass) under normal ECS conditions. By contrast, cells that expressed the wild-type Cx30 protein did not take up the dextran–rhodamine dye in ECS (Fig. 5C). Collectively, these studies indicate that the V37E and G59R mutants are loss-of-function mutants, whereas the T5M mutant shows similar functional channel properties to the wild-type Cx30 protein.

Journal of Cell Science (2014) 127, 1751–1764 doi:10.1242/jcs.138230

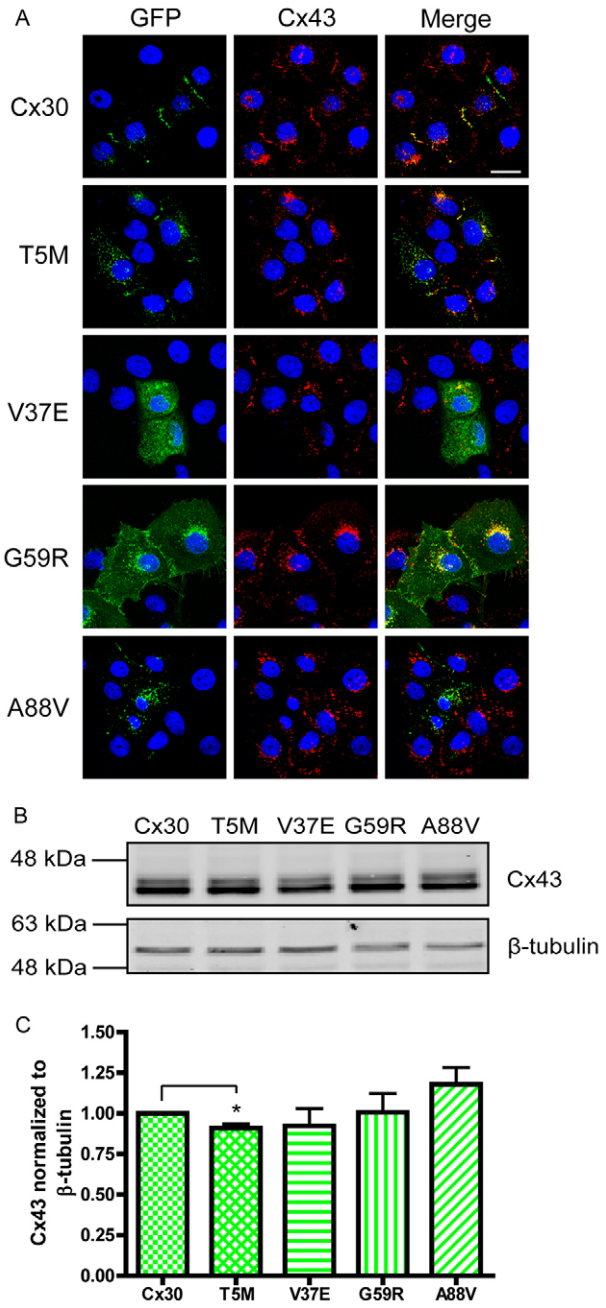

Fig. 3. The effect of Cx30 mutants on endogenous Cx43 in REKs. (A) Cx30- and Cx30-mutant-expressing REKs (green) were immunolabeled for Cx43 (red) and stained with Hoescht 33342 (blue) to denote cell nuclei. Cx43 plaques were localized at the cell surface between REKs expressing wild-type Cx30 or the T5M and G59R mutants. V37E- and A88V-expressing REKs did not exhibit Cx43 plaque formation between apposing cells. Scale bar: 20 μm. (B) Western blot analysis was used to detect the total levels of Cx43 in Cx30- and mutant-expressing cells when normalized to β-tubulin. (C) Total levels of Cx43 were slightly lower in REKs expressing only the T5M mutant that is associated with hearing loss. Total levels of Cx43 remained unchanged in cells that expressed the V37E, G59R and A88V mutant Cx30 proteins. Values represent the mean fold change±s.e.m., *$P<0.05$, unpaired Student's *t*-test, $n=3$.

The A88V mutant caused membrane disruption and cell death 24 hours after expression, therefore hemichannel status could not be assessed.

The V37E and A88V mutants induce apoptosis through distinct mechanisms

The ectopic expression of the V37E and A88V mutants induced some degree of cell death in REKs as early as 18 hours post-expression, with the majority of A88V-expressing cells dying within 48 hours (data not shown). To determine the mechanism of cell death induced by these mutants, control and mutant-expressing REKs were immunolabeled with an antibody against cleaved caspase-3, a marker of the committed stage of apoptosis (Saraste and Pulkki, 2000). Interestingly, some V37E- and A88V-expressing REKs exhibited cleaved caspase-3, indicating that these cells were undergoing apoptosis (supplementary material Fig. S2). To further validate and quantify this finding, terminal deoxynucleotidyl transferase dUTP nick end labeling (TUNEL) assays, which measure the degradation stage of apoptosis (Saraste and Pulkki, 2000), were performed on Cx30- and mutant-expressing REKs. Expression of the V37E and A88V Cx30 mutants significantly induced apoptosis, as ~70% and ~80% of GFP-expressing cells, respectively, were ApopTag positive (***$P<0.001$) compared with GFP only REKs, of which only ~2% were ApopTag positive (Fig. 6A,B). Untransfected cells that had been treated with staurosporine (Stauro) for 24 hours served as a positive control for the assay – ~90% of the total cells were apoptotic in comparison with untransfected controls (***$P<0.001$, Fig. 6C).

Because some of the mutants localized to the ER, we wanted to determine whether apoptosis was induced by an ER-stress-mediated UPR. Western blot analyses of REK cell lysates were performed to detect changes in the levels of markers that are involved in different stages and pathways of the UPR. REKs that had been treated with tunicamycin, an inducer of ER stress that blocks N-glycosylation of proteins (de Freitas et al., 2011), served as positive controls for UPR markers. When compared with GFP-expressing cells, expression of the ER lumenal chaperone GRP78 (also known as HSPA5) was not elevated in cells that expressed the mutant Cx30 proteins (supplementary material Fig. S3A). The activating transcription factor 4 (ATF4) was upregulated to a small extent in cells that expressed only the V37E mutant (***$P<0.001$) (supplementary material Fig. S3B). Finally, the C/EBP homologous protein (CHOP, also known as DDIT3) was not elevated in cells that expressed any of the mutants when compared with GFP-expressing control cells and only significantly increased in cells that had been treated with tunicamycin (supplementary material Fig. S3C).

To determine whether expression of the Cx30 V37E mutant activates the IRE1 arm of the UPR, we performed an X-box binding protein 1 (XBP1) splicing assay (Calfon et al., 2002; Williams and Lipkin, 2006). In response to unfolded proteins, IRE1 directly splices a small intron from XBP1 mRNA (Ron and Walter, 2007), which contains a single *Pst*I restriction site (supplementary material Fig. S3D–G). Agarose gel analysis of XBP1 cDNA confirmed the presence of the unspliced product in untransfected controls, as shown by the doublet band at ~300 bp (XBP1u) and low expression of the spliced 575-bp band (XBP1s) after digestion of the cDNA with *Pst*I (supplementary material Fig. S3F). The tunicamycin control had elevated levels of undigested cDNA (575 bp) and a complete loss of the unspliced fragments (XBP1u), suggesting that the majority of XBP1 mRNA had been spliced. In comparison with the untransfected control, wild-type Cx30 and the T5M, V37E, G59R and A88V mutants displayed no discernible differences in XBP1 splicing (supplementary material Fig. S3F). Detailed images of the bands that migrated more slowly (supplementary material Fig. S3F) revealed a small increase in XBP1s (575 bp) in comparison with XBP1u (601 bp) for

Journal of Cell Science (2014) 127, 1751–1764 doi:10.1242/jcs.138230

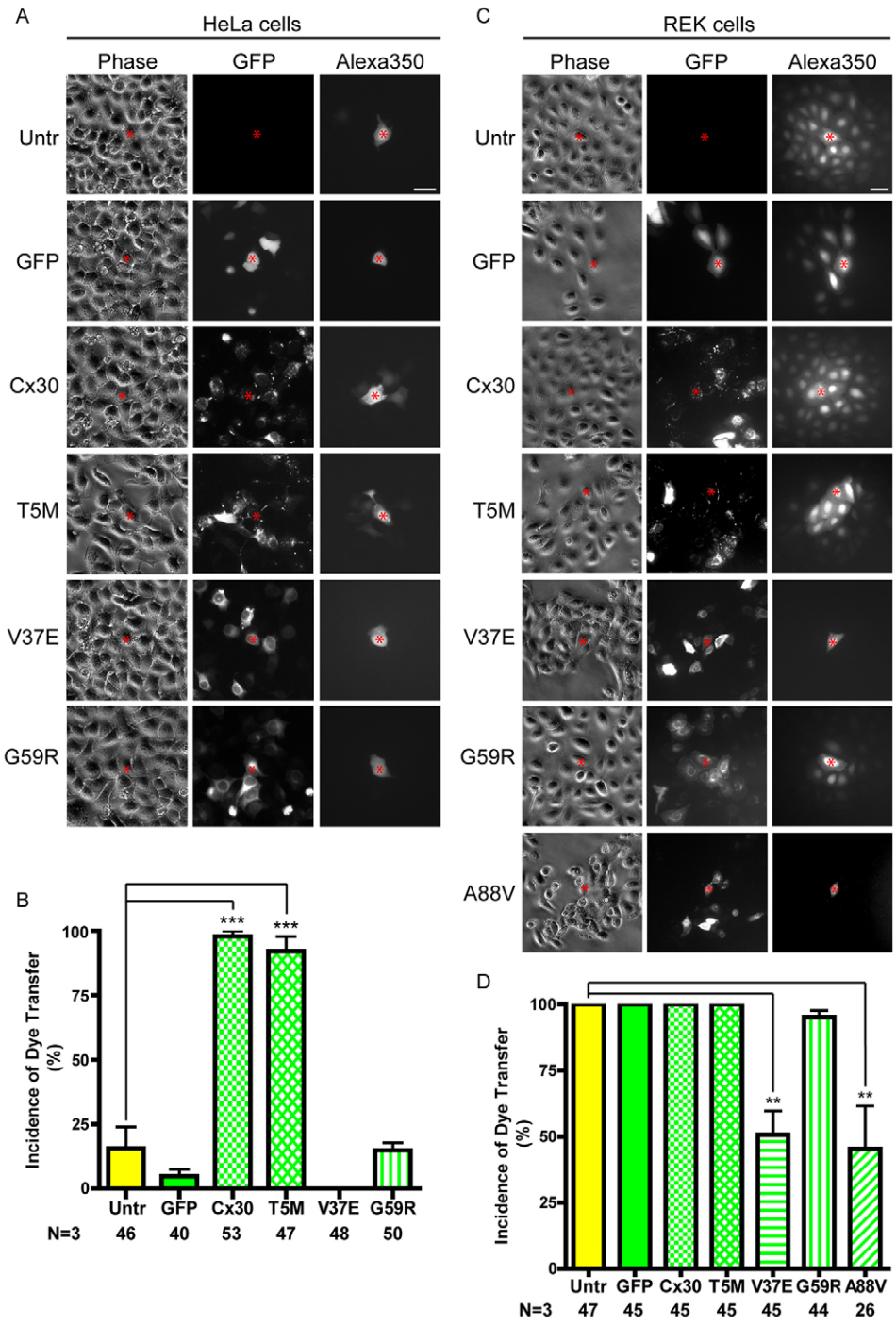

Fig. 4. The V37E, G59R and A88V mutants that are linked to skin disease affect GJIC when expressed in HeLa cells and REKs. (A) HeLa cells expressing GFP, wild-type Cx30 or the indicated mutant proteins were imaged for the presence of GFP and then microinjected with Alexa-Fluor-350 dye (red asterisks). (B) Relative to untransfected (Untr) control cells, cells expressing Cx30 or the T5M mutant exhibited a significantly greater incidence of dye transfer than those expressing the V37E or G59R mutants. (C) Untransfected and GFP-, Cx30- and mutant-expressing REKs were imaged for the presence of GFP and then microinjected with Alexa-Fluor-350 dye (red asterisks). (D) Relative to untransfected controls, cells expressing the V37E and A88V mutants exhibited significantly lower incidences of Cx43-mediated dye transfer. (B, D). Values represent the mean percent incidence of dye transfer±s.e.m., $^{**}P<0.01$, $^{***}P<0.001$, one-way ANOVA, $n=3$). The numbers of cells that were injected are presented along the bottom of the figures. Scale bars: 20 μm.

transfected cells, but this was most probably a result of protein overexpression. The ratio of the 575-bp band to the ~300-bp doublet band showed that only the tunicamycin control significantly induced splicing of XBP1 mRNA (supplementary material Fig. S3G, $^{***}P<0.001$, $n=6$), suggesting that the V37E mutant does not induce an IRE1-mediated UPR.

The V37E and A88V mutants might exhibit dominant-negative and trans-dominant effects on wild-type Cx30 and Cx26 when coexpressed in REKs

To determine whether localization of the Cx30 mutants that are linked to skin disease and retained in intracellular compartments could be rescued (to the cell surface), REKs were engineered to express Cx30–RFP or Cx26–RFP simultaneously with GFP-tagged Cx30 mutants. Alone, Cx30–RFP formed gap junctions (Fig. 7), which also facilitated the transfer of Alexa Fluor 350 in HeLa cells and REKs (data not shown). Cx30–GFP and T5M–GFP showed distinct colocalization with Cx30–RFP, with limited intracellular localization, whereas wild-type Cx30 did not appear to rescue localization of the V37E mutant to the cell surface (Fig. 7). Although the G59R and A88V mutants showed some colocalization with wild-type Cx30 at the cell surface, a considerable amount of these mutant proteins was localized in intracellular compartments, indicating that coexpression with

Journal of Cell Science (2014) 127, 1751–1764 doi:10.1242/jcs.138230

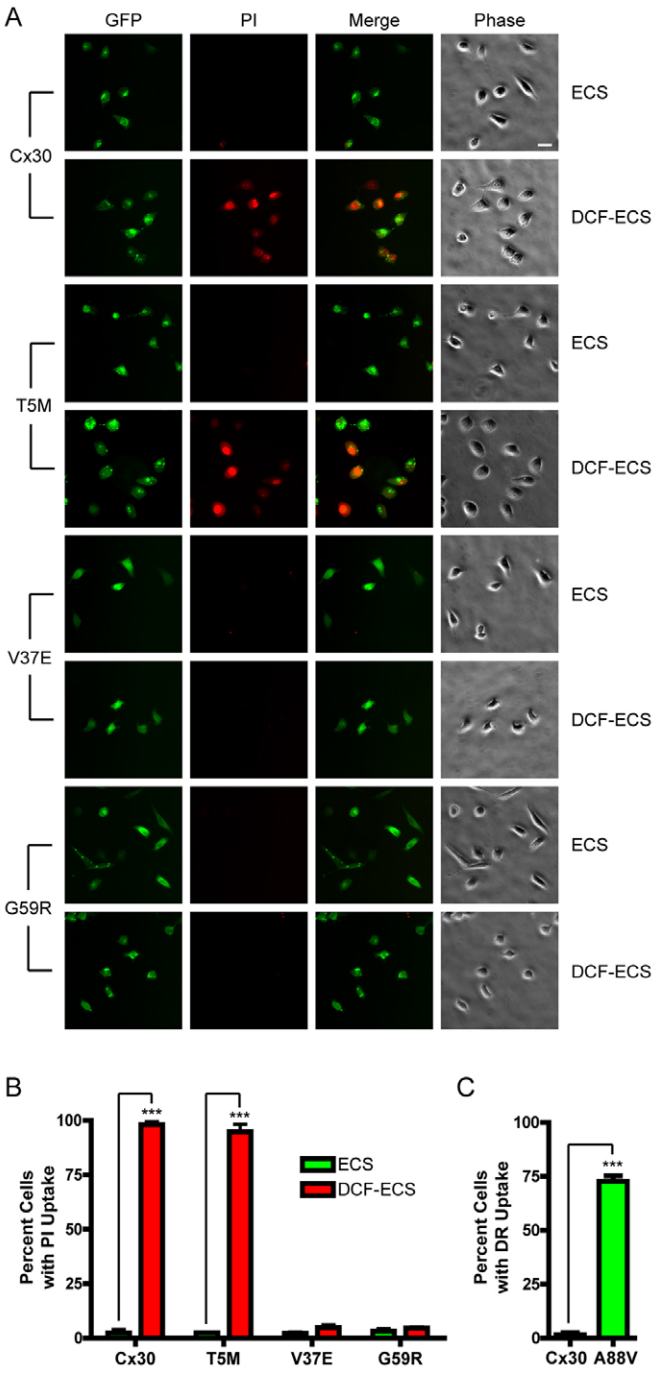

Fig. 5. The hearing-loss-linked T5M mutant exhibits hemichannel activity in HeLa cells that mimics Cx30. (A) Single isolated HeLa cells that expressed the wild-type Cx30 or indicated mutant proteins were incubated with propidium iodide (PI) in normal extracellular solution (ECS) or divalent-cation-free ECS (DCF-ECS). Cells were imaged for the presence of GFP (green) and PI uptake (red). Scale bar: 20 µm. (B) Cells that expressed the V37E and G59R mutants did not take up PI under DCF-ECS conditions, whereas those expressing Cx30 or the T5M mutant exhibited significant hemichannel activity. Values represent the mean percentage of GFP-positive isolated cells that exhibited PI uptake±s.e.m., ***$P<0.001$, two-way ANOVA, $n=4$. (C) The majority of single cells that expressed the A88V mutant were permeable to dextran–rhodamine (DR) under ECS conditions, indicating disruption of the cell membrane. Thus, the A88V mutant could not be used in the PI uptake assay. Values represent the mean percentage of GFP-positive isolated cells that exhibited DR uptake±s.e.m., ***$P<0.001$, Student's *t*-test, $n=3$.

wild-type Cx30 was not sufficient to fully rescue the trafficking of Cx30 mutants to the cell surface (Fig. 7). Notably, the V37E and A88V mutants might exhibit partial dominant-negative effects on wild-type Cx30, because a large amount of Cx30–RFP was retained inside the cell when compared with cells where Cx30–RFP was expressed alone (Fig. 7). In particular, the A88V mutant and wild-type Cx30 protein exhibited colocalization in a distinct subcellular compartment. We also observed similar results in HeLa cells, whereby the V37E, G59R and A88V mutants all exhibited small amounts of colocalization with wild-type Cx30 at the cell surface, but a substantial amount of the mutant protein was localized intracellularly (supplementary material Fig. S4). Alone, Cx26–RFP formed gap junctions in REKs (Fig. 8). Cx30–GFP, T5M–GFP and G59R–GFP also showed colocalization with Cx26–RFP; however, the V37E and A88V mutants, and a considerable amount of the G59R mutant protein remained within intracellular compartments, indicating that wild-type Cx26 did not rescue the trafficking of these mutants (Fig. 8). It is possible that the V37E and A88V mutants also exhibit trans-dominant effects on Cx26, as the majority of Cx26–RFP was retained inside the cell compared with when Cx26–RFP was expressed alone (Fig. 8). Again, similar results were also obtained in HeLa cells that had been engineered to coexpress wild-type Cx30 or Cx30 mutants with Cx26–RFP. Wild-type Cx30 and the T5M mutant showed strong colocalization at gap junction plaques (supplementary material Fig. S4). The G59R mutant also colocalized strongly with Cx26–RFP at gap junction plaques, but a population of the mutant protein remained within intracellular compartments. The V37E mutant appeared to have trans-dominant effects on Cx26–RFP because, upon coexpression with this mutant, less Cx26–RFP was identified in plaques, whereas some A88V could traffic to the cell surface with Cx26–RFP (supplementary material Fig. S4).

DISCUSSION

In the present study, we first determined that the T5M mutant, which is linked to non-syndromic hearing loss, exhibited similar properties to wild-type Cx30 as it formed functional gap junctions and hemichannels. The mutants that are associated with skin disease exhibited impaired gap junction formation and function. In particular, the V37E mutant, which is linked to KID syndrome, was retained in the ER and induced apoptosis, leading to the hypothesis that this was occurring through the UPR. However, only the ATF4 UPR marker was elevated to a small degree in cells that expressed this mutant, with all other indices of activation of the UPR remaining unchanged. This suggests that cell death was probably triggered by a UPR-independent mechanism. By contrast, the G59R mutant, which is associated with Vohwinkel and Bart-Pumphrey syndromes, was primarily retained in the Golgi apparatus and did not induce cell death. The A88V mutant, which is linked to Clouston syndrome, remained, primarily, in intracellular compartments but could be trafficked to the cell surface. Nevertheless, it potently induced apoptosis, possibly through mechanisms that include leaky hemichannels that might form within an intracellular compartment or at the cell surface. Finally, we determined that the retention in intracellular compartments of the mutants that are linked to skin disease could not be overcome upon coexpression with Cx43, Cx30 or Cx26, and that the V37E and A88V mutants exhibited dominant-negative and trans-dominant effects on the trafficking of the wild-type connexins to the cell surface. Thus, we clearly demonstrate the complexity of connexin-linked diseases, as each Cx30 mutant

Journal of Cell Science (2014) 127, 1751–1764 doi:10.1242/jcs.138230

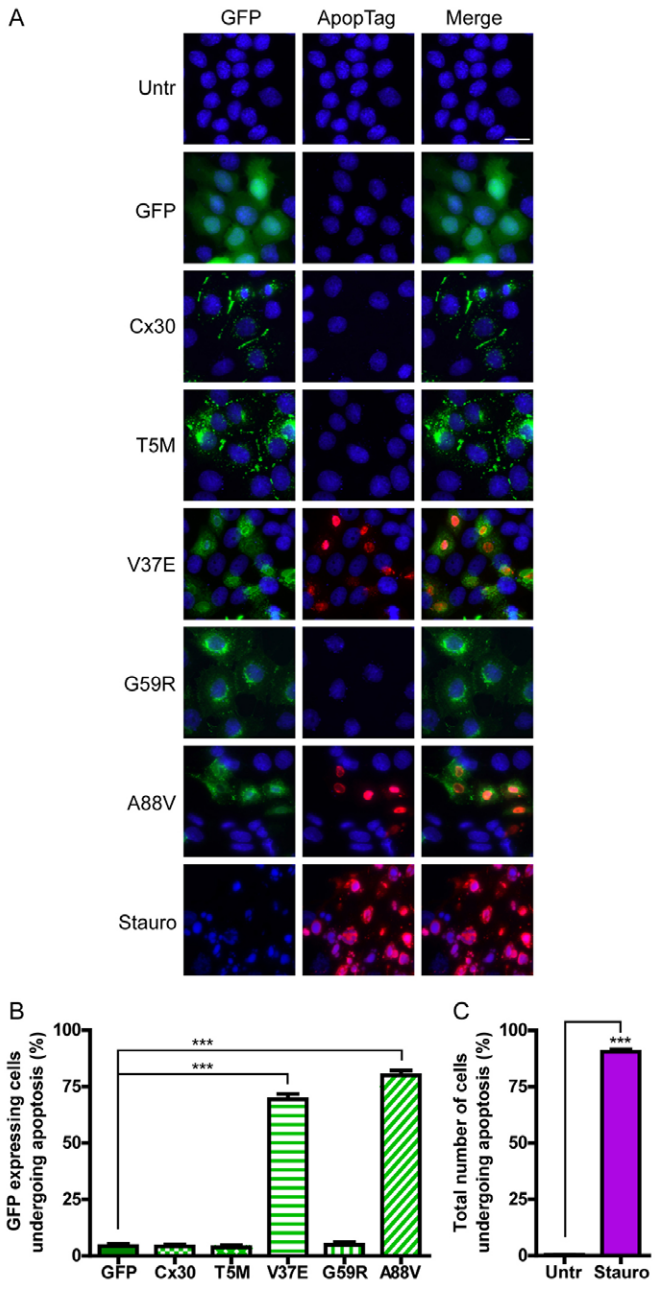

Fig. 6. Ectopic expression of the V37E and A88V mutants that are associated with Clouston syndrome induces apoptosis in REKs. (A) TUNEL assays were performed on untransfected (Untr), GFP-, Cx30- and mutant-expressing REKs (green). Nuclei were stained with Hoescht 33342 (blue) and apoptotic cells are indicated by ApopTag staining (red). Cells that had been treated with Staurosporine (Stauro), an inducer of apoptosis, were used as controls. Scale bar: 20 μm. (B) The expression of the V37E and A88V mutants significantly induced apoptosis in REKs. (C) Treatment with staurosporine significantly induced apoptosis compared with untransfected controls. The values represent apoptotic cells as the mean percentage of the total number of cells per image±s.e.m., ***$P<0.001$, one-way ANOVA, $n=3$.

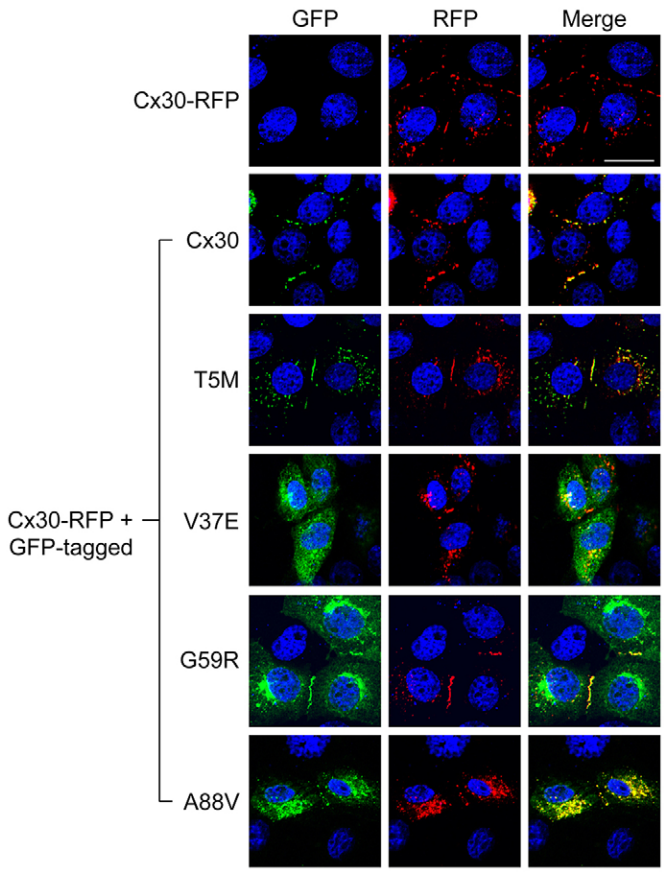

Fig. 7. Cx30 has minimal ability to rescue the trafficking of skin-disease-linked mutants to the cell surface in REKs. REKs that coexpressed Cx30–RFP (red) together with the indicated GFP-tagged Cx30 constructs (green) were stained with Hoescht 33342 (blue) to label the cell nuclei. Cx30, the T5M mutant and some of the G59R and A88V mutant proteins distinctly colocalized with Cx30–RFP at the cell surface. Wild-type Cx30 minimally rescued the trafficking of V37E, G59R and A88V mutants because a substantial amount of the protein was localized to intracellular compartments. Colocalization is indicated in the merged images (yellow). Scale bar: 20 μm.

exhibited markedly different characteristics and trans-dominant properties within cells. These findings also show that the disease phenotype correlates with the severity of the effects of the mutant proteins on cellular health and overall GJIC.

In order to evaluate the link between Cx30 mutants and disease, we used spontaneously immortalized newborn REKs, which have previously been reported to express mRNA for nine connexins – including Cx30 (Maher et al., 2005) – and are phenotypically similar to basal keratinocytes given their ability to differentiate and stratify (Langlois et al., 2007; Maher et al., 2005; Thomas et al., 2007). At the protein level, REKs abundantly express Cx43 and only express Cx26 upon differentiation (Maher et al., 2005). The fact that REKs do not express detectable levels of Cx30 in monolayer cultures allowed us to express and track both GFP-tagged and untagged variants of Cx30 and the mutants. Similar localization profiles and function were observed for all GFP-tagged and untagged wild-type Cx30 and Cx30 mutants, strongly suggesting that the fusion of GFP on the C-terminal tail did not affect the properties of Cx30, similar to previous reports for Cx26 (Marziano et al., 2003) and Cx43 (Jordan et al., 1999).

The T5M mutant, linked to non-syndromic hearing loss

The T5M mutant is one of only two Cx30 mutants that are linked specifically to non-syndromic hearing loss (Grifa et al., 1999;

Journal of Cell Science (2014) 127, 1751–1764 doi:10.1242/jcs.138230

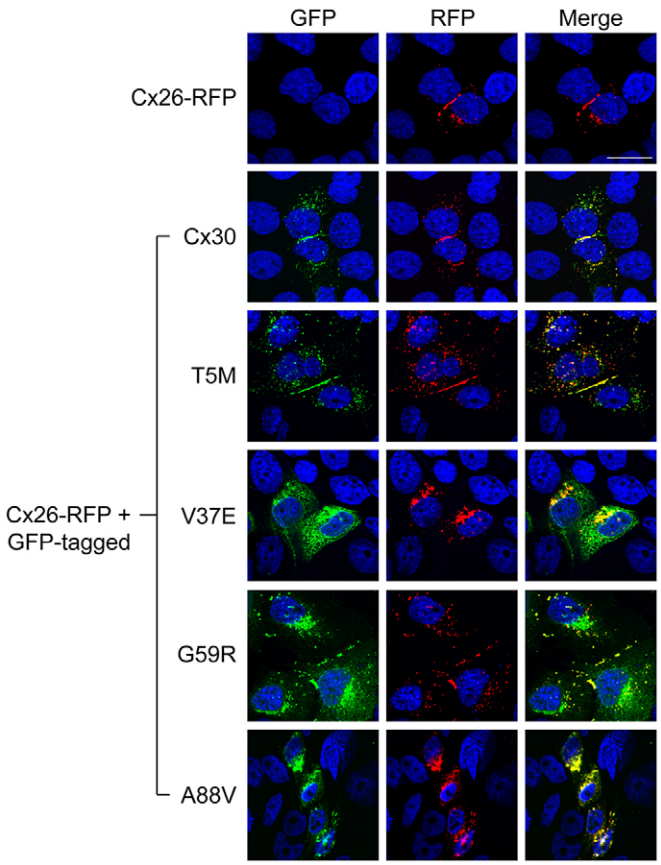

Fig. 8. Cx30 mutants linked to Clouston syndrome exhibit a dominant-negative effect on ectopically expressed Cx26 in REKs. REKs coexpressing Cx26–RFP (red) together with GFP-tagged wild-type Cx30 or the indicated mutants (green) were stained with Hoescht 33342 (blue) to stain the cell nuclei. Wild-type Cx30, the T5M mutant and some of the G59R mutant distinctly colocalized with Cx26–RFP at the cell surface. Wild-type Cx26 failed to rescue the trafficking of V37E and A88V mutants, whereas a substantial amount of the G59R mutant protein accumulated within intracellular compartments. The V37E and A88V Cx30 mutants exhibited a dominant-negative effect on wild-type Cx26, as Cx26–RFP was retained inside the cell and, notably, colocalized with the A88V mutant. Colocalization is indicated in the merged images (yellow). Scale bar: 20 μm.

Wang et al., 2011). Consistent with our results, the T5M mutant has been previously found to form gap junctions (Common et al., 2002); however, its functional capacity remains controversial. *In vitro* electrophysiological studies have previously shown that the T5M amino acid substitution drastically reduced electrical coupling between *Xenopus laevis* oocytes (Grifa et al., 1999), whereas other reports have shown restrictions in the trans-junctional molecules that can pass through T5M channels (Common et al., 2002; Schütz et al., 2010; Zhang et al., 2005). In our study, we found that both T5M-based hemichannels and gap junction channels were functional, allowing the passage of sizable molecules – e.g. prodium iodide, Alexa Fluor 350 – in mammalian cells, raising the question as to why this mutant causes hearing loss.

The answer might be linked to subtle changes in the N-terminal domain of Cx30 where the substitution of methionine for threonine occurs. Cx30 shares 76% sequence identity with Cx26 (Grifa et al., 1999), and although the crystal structure of Cx30 has not yet been resolved, the crystal structure of Cx26 has elucidated that the N-terminal tail lines the gap junction channel pore, creating a funnel that restricts channel selectivity based on molecular size, flexibility, charge and charge distribution (Harris, 2007; Kwon et al., 2011; Maeda et al., 2009). In the nonsensory cells of the inner ear, Cx26 and Cx30 intermix to form heteromeric and heterotypic channels (Ahmad et al., 2003; Forge et al., 2003; Marziano et al., 2003; Yum et al., 2007) and are suggested to form functional hemichannels (Gossman and Zhao, 2008; Zhao et al., 2005). Through extrapolation, mutation of the highly conserved hydrophilic T5 amino acid residue in Cx30 (Grifa et al., 1999) could alter the permeability properties of both homotypic Cx30 and heterotypic Cx26–Cx30 channels. Another possibility might be how the T5M mutant affects Cx26, because the role of Cx30 in hearing remains controversial (Boulay et al., 2013; Miwa et al., 2013; Teubner et al., 2003) and increasing evidence suggests that Cx26 and Cx30 are co-regulated (Boulay et al., 2013). Expression levels of Cx26 are dramatically reduced upon Cx30 knockout (Boulay et al., 2013) and in Cx30 T5M knock-in mice that also exhibit decreased levels of Cx30 (Schütz et al., 2010). Importantly, in the inner ear, this mutant might be affecting Cx26 levels, potentially reducing the frequency of heteromeric and heterotypic channel formation that is necessary for K^+ buffering. In addition, Cx30 has been reported to be involved in glucose uptake and metabolic coupling between mouse cochlear cells (Chang et al., 2008). Therefore, the T5M mutation, although able to pass ions and molecular dyes, might reduce, but not inhibit, the permeability of metabolites, such as glucose, between supporting cells in the avascular sensory epithelium. However, further investigation is necessary to clearly understand how the T5M mutation has such effects.

Our finding that T5M gap junction channels and hemichannels are functional agrees, in part, with other findings that suggest ionic permeability is not affected by this amino acid replacement (Schutz et al., 2010; Zhang et al., 2005). However, larger molecules, such as propidium iodide (Zhang et al., 2005), inositol trisphosphate (IP3) and calcein (Schütz et al., 2010), have been reported to have reduced permeability. The intercellular transfer of calcein and IP3 was observed between cells that had been obtained from organotypic cochlear cultures from $Cx30^{T5M/T5M}$ mice, where Cx26 is also known to be coexpressed. Thus, the presumed heteromeric conformation of channels comprising the T5M Cx30 mutant and wild-type Cx26 proteins might have an overriding effect on channel permeability and selectivity in comparison with homomeric T5M channels. However, the ability of the T5M mutant to take up propidium iodide and transfer Alexa 350 in our study contrasts with studies by Zhang and colleagues, and by Common and colleagues, respectively (Zhang et al., 2005; Common et al., 2002). We can only speculate on this issue and suggest that it might be due to differences in the linker sequences that fuse the T5M mutant to GFP or to differences in species sequences. Nevertheless, the fact that the T5M mutant is functional has been thoroughly established, suggesting that disease is probably linked to more subtle changes in channel regulation or changes in the structure of the N-terminus.

The loss-of-function V37E mutant, linked to Clouston and KID syndromes

Although previously considered to be linked distinctly to Clouston syndrome (Common et al., 2002; Smith et al., 2002), the V37E mutant has now also been implicated in KID syndrome (Jan et al., 2004). Other than the fact that the V37E mutant is retained in an unknown intracellular compartment (Common

Journal of Cell Science (2014) 127, 1751–1764 doi:10.1242/jcs.138230

et al., 2002), little was known about this mutant. Here, we conclusively show that the V37E mutant is retained within the ER where it is surveyed by molecular machinery as part of cellular quality control (Kleizen and Braakman, 2004). Furthermore, this mutant, which exhibits loss of hemichannel and gap junction channel function, acted in a (trans)dominant-negative fashion on coexpressed Cx43, Cx26 and Cx30 and significantly induced apoptosis in REKs.

The V37E mutant is positioned in the first transmembrane domain of Cx30. According to the crystal structure of Cx26, the first transmembrane domain is the major pore-lining helix that is involved in prominent intraconnexin interactions with all other transmembrane domains to stabilize the basic structure of the connexin subunit (Maeda et al., 2009). In addition, the V37 amino acid is located in a motif, ^{37}VVAA^{40}, that is conserved between Cx26 and Cx30 (Maeda et al., 2009; Smith et al., 2002), and, as demonstrated by the V37I Cx26 mutant, mutations within this particular motif reduce hexamer formation and channel function (Jara et al., 2012). Importantly, the V37E Cx30 mutation involves a unique and crucial substitution of a glutamic acid residue for a hydrophobic valine, which we propose alters crucial intraconnexin interactions and Cx30 stability, resulting in improper folding and protein accumulation in the ER. In addition, various Cx26 mutants that are linked to Vohwinkel syndrome and PPK have been reported to exhibit dominant-negative and trans-dominant effects on other connexins, including Cx30 and Cx43 (Forge et al., 2003; Marziano et al., 2003; Rouan et al., 2001). V37E Cx30 might exhibit these effects on coexpressed wild-type Cx30, Cx26 and Cx43, although, it is also possible that V37E-mutant expressing cells undergoing apoptosis internalize these connexins, as has been reported for Cx43 (Kalvelyte et al., 2003).

When the V37E mutant was expressed in keratinocytes, it induced apoptotic cell death that we hypothesized might occur through the UPR. The UPR is a protective cellular mechanism that is regulated by the lumenal ER chaperone GRP78 (Malhotra and Kaufman, 2007) and is involved in normal keratinocyte differentiation (Sugiura et al., 2009), as well as normal lens development (Alapure et al., 2012). Of note, mutations in Cx31 and Cx50, which are linked to erythrokeratoderma variabilis (EKV) and cataracts, respectively, induce an abnormal ER-stress-mediated UPR (Alapure et al., 2012; Tattersall et al., 2009) and result in extensive cell death (Di et al., 2002; He et al., 2005). Although the expression of the V37E Cx30 mutant did not induce the upregulation of GRP78, which might occur upon the activation of the activating transcription factor 6 (ATF6) pathway (Berridge, 2002), the V37E mutant only moderately induced the expression of ATF4. ATF4 activates cell-death-initiating caspases, including caspase 3, through the mitochondria-dependent intrinsic cell death pathway (Galehdar et al., 2010; Groenendyk and Michalak, 2005; Malhotra and Kaufman, 2007). By contrast, the ER-stress-induced splicing of XBP1 through activation of IRE1 did not occur in cells that expressed the V37E mutant, suggesting that the mechanism of cell death might be independent of the UPR. This was somewhat surprising because the V37E mutant clearly accumulated in the ER and initiated apoptosis. However, evidence exists to suggest that misfolded secretory proteins, such as an α_1-antitrypsin Z mutant, can accumulate in the ER, induce ER vesiculation and activate caspase-dependent pathways without activating the UPR (Hidvegi et al., 2005). In addition, NFκB activation and Ca^{2+} release from the ER through an alternative ER overload response (EOR) pathway have also been demonstrated to be distinct from the UPR (Pahl et al., 1996). Various stresses, such as changes in ER Ca^{2+} (Subramanian and Meyer, 1997), can alter ER structure in a similar manner, but the functional relevance of these alterations is unclear. Whether the V37E mutant is causing cell death through these alternative UPR-independent pathways remains to be determined, but the short time frame and rapid activation of apoptosis makes further dissection of the mechanisms involved difficult to ascertain.

The loss-of-function G59R mutant, linked to Vohwinkel/Bart-Pumphrey syndromes

Here, a previously uncharacterized loss-of-function Cx30 G59R mutant was found to occasionally form gap junction plaques, but was mainly localized to the Golgi apparatus. This is consistent with findings for the G59A and D66H Cx26 mutants that are linked to Vohwinkel syndrome (Bakirtzis et al., 2003; Marziano et al., 2003; Thomas et al., 2004), suggesting that mutations in the first extracellular domain of Cx30 and Cx26 might lead to similar disease phenotypes. Supporting an essential role for the first extracellular loop, the N45K Cx26 mutation located in this domain causes Bart-Pumphrey syndrome (Richard et al., 2004). The evolutionarily conserved first extracellular loop of Cx26 (and by extension Cx30) has been suggested to play a role in voltage gating (Tang et al., 2009; Verselis et al., 2009), and, more importantly, interconnexin and interconnexon interactions (Maeda et al., 2009). Therefore, the Cx30 G59R mutant might result in defective connexin oligomerization, which occurs primarily in the ER and Golgi apparatus for several connexins – including Cx32, Cx26, Cx43 and Cx46 (Das Sarma et al., 2002; Evans et al., 1999; Koval et al., 1997; Musil and Goodenough, 1993). Reduced channel function at the cell surface might also indicate defective hemichannel docking, highlighting the importance of this domain in channel formation and function, which are compromised in hearing loss and skin diseases.

The A88V mutant, linked to Clouston syndrome

The A88V mutant is one of four mutants that are linked to Clouston syndrome. Previous studies have localized the A88V mutant to intracellular compartments, and localization of this mutant could be partially rescued to the cell surface upon coexpression with wild-type Cx30 (Common et al., 2002; Essenfelder et al., 2004). The A88V mutant was also found to exhibit abnormal hemichannel activity, which causes ATP release and subsequent cell death (Essenfelder et al., 2004). We extended these studies by demonstrating that a proportion of the A88V mutant population also formed gap-junction-like structures and negatively affected Cx43-based gap junction coupling and the trafficking of both wild-type Cx26 and Cx30. These dominant-negative and trans-dominant effects might be associated with the fact that the A88V mutant significantly induced apoptosis in REKs, similar to our discussion above of the V37E mutant.

Clearly, the A88 amino acid residue is crucial for Cx30 hemichannel and channel function. Cx30 forms voltage-gated hemichannels (Valiunas and Weingart, 2000), which are normally closed under physiological conditions and open in response to low extracellular concentrations of Ca^{2+} and Mg^{2+} (De Vuyst et al., 2007; Tong et al., 2007; Verselis and Srinivas, 2008). Importantly, leaky hemichannels that result in cell death have been reported for a number of other connexin mutations (Gerido et al., 2007; Lee et al., 2009; Mese et al., 2011; Stong et al., 2006) and also for the A88V Cx26 mutation, which is linked to KID syndrome (Mhaske et al., 2013). The crystal structure of Cx26 suggests that part of the

second transmembrane domain also lines the channel pore and is involved in intraconnexin interactions with other domains, including the N-terminus, that dictate specific protein conformation (Kwon et al., 2011; Maeda et al., 2009). By analogy, it is possible that the A88V Cx30 mutation affects protein folding and stability, and alters important interactions, moving the N-terminal domain away from the cytoplasmic entrance of the pore (Kwon et al., 2011; Maeda et al., 2009) to favor abnormal hemichannel activity. Therefore, we propose that leaky A88V Cx30 hemichannels contribute to the induction of apoptosis in REKs. Because Cx30 probably oligomerizes in the early stages of the secretory pathway, leaky A88V hemichannels (or connexons) could disrupt the Ca^{2+} gradient in the ER and other compartments, possibly triggering a rapid cell death response.

In conclusion, the present study characterizes four Cx30 mutations that are linked to skin disease (A88V), hearing loss (T5M) and combinations of both (V37E and G59R). Each mutation results in disease manifestation through distinct mechanisms, ranging from a mutant that exhibits wild-type Cx30 characteristics (T5M) to mutants that induce apoptosis through possible constitutive and premature activation of hemichannels, or through ER signaling mechanisms that are UPR-independent (A88V, V37E). Moreover, the loss-of-function G59R mutant causes yet another skin disease phenotype that manifests as a combination of Vohwinkel and Bart-Pumphrey syndromes. All of these Cx30 autosomal dominant gene mutations cause syndromic and non-syndromic disease through different mechanisms and future studies will need to determine the key roles of co-regulated connexins in the cochlea and epidermis.

MATERIALS AND METHODS

Generation of cDNA constructs

Mouse Cx30 cDNA encoded within the pBluescript vector, kindly provided by Christian C. Naus (University of British Columbia, Vancouver, Canada), was cloned into a pEGFP expression vector using the *Xho*I and *Not*I restriction enzymes. This combination of restriction enzymes removed the enhanced GFP (eGFP) cDNA from the vector as described by Thomas and colleagues (Thomas et al., 2004). Cx30 mutants were constructed using the QuikChange site-directed mutagenesis kit (Stratagene, La Jolla, CA) as per the manufacturer's instructions. The following primer pairs were used to create the Cx30 mutations. The nucleotide change is underlined in each case: T5M sense, 5′-GCACGATGGACTGGGGGATGCTGCACACCGTCA-TCGG-3′; antisense, 5′-CCGATGACGGTGTGCAGCATCCCCCAGT-CCATCGTGC-3′; V37E, sense, 5′-CCGAGTCATGATCCTAGAG-GTGGCTGCCCAG-3′; antisense, 5′-CTGGGCAGCCACCTCTAGGA-TCATGACTCGG-3′; A88V, sense, 5′-CTTTGTGTCTACCCCAGTC-CTGTTGGTGGCCATGC-3′; antisense, 5′-GCATGGCCACCAACAG-GACTGGGGTAGACACAAAG-3′. The Cx30 G59R mutant was purchased from Norclone Biotech Laboratories (London, Ontario, Canada). To ensure that only the mutation of interest had been introduced, all constructs were sequenced.

To create GFP-tagged constructs and Cx30–RFP, PCR was performed to introduce *Xho*I and *Eco*RI restriction sites to the 5′ and 3′ ends of the wild-type Cx30 and Cx30 mutant sequences, respectively, and to remove the stop codon to allow for the expression of GFP. Following digestion with *Xho*I and *Eco*RI restriction enzymes, the PCR products were cloned into the pEGFP-N1 (Clontech, Palo Alto, CA) and pTagRFP-N (Evrogen; distributed by Cedarlane, Burlington, Ontario, Canada) vectors to produce GFP-tagged constructs and Cx30–RFP, respectively. Cx43–mRFP was kindly provided by Guido Gaietta (University of California, San Diego, CA) and has been described previously (Gong et al., 2007). For construction of the vector encoding Cx26–RFP, restriction digest of a vector encoding Cx26 fused to the yellow fluorescent protein (Laird et al., 2001) was performed, by using *Xho*I and *Eco*RI, to isolate Cx26 cDNA, which was then directly subcloned into the pTagRFP-N vector as described above. All constructs were confirmed by sequencing.

Cell culture and transient transfections

GJIC-competent REKs, kindly provided by Vincent C. Hascall (Cleveland Clinic, Cleveland, OH), and communication-deficient HeLa cells (ATCC, Manassas, VA) were cultured in high glucose Dulbecco's modified Eagle's medium (DMEM) that was supplemented with 10% fetal bovine serum, 100 U/ml penicillin, 100 µg/ml streptomycin and 2 mM L-glutamine (Invitrogen, Burlington, ON), in a humidified incubator maintained at 37℃ under 5% CO_2 as previously described (Maher et al., 2005). Cells were passaged once they reached 80–100% confluence using 0.25% trypsin-EDTA (Invitrogen) and were cultured in 35-mm or 60-mm plastic tissue culture dishes for all experimental procedures. Before transfection, all cells were grown to 65–80% confluence, and those that were to be used for immunolabeling or TUNEL assays were also grown on glass coverslips. Cells were transfected with 2–6 µg of DNA by using Lipofectamine 2000 (Invitrogen) in the presence of low serum OptiMEM medium (Invitrogen), as previously described (Penuela et al., 2007), or by using the JetPRIME-mediated transfection kit (VWR International, Mississauga, Ontario, Canada) according to the manufacturer's instructions. As controls, untransfected cells were exposed to the transfection reagents and the appropriate media without the addition of any DNA. As a second control, a population of cells was also transfected with a vector encoding free GFP. Co-transfections were performed using the Polyplus JetPRIME transfection method by mixing 1 µg of Cx30– or Cx26–RFP and 1 µg of each GFP-tagged Cx30 mutant. All transfections were terminated after 24 hours. Positive controls for the induction of ER stress or apoptosis included cells that were plated in parallel, treated for 24 hours with 2 µg/ml tunicamycin or 0.5 µg/ml staurosporine, respectively (both from Sigma-Aldrich, St Louis, MO).

Immunocytochemistry

Cells that had been grown in a monolayer on glass coverslips were fixed with 10% neutral buffered formalin (NBF) (EMD Millipore, Billerica, MA) for 25 minutes at room temperature. In a humidified chamber, fixed cells were blocked for 30–45 minutes at room temperature in PBS containing 2% bovine serum albumin (Santa Cruz Biotechnology, Dallas, TX), to prevent non-specific antibody binding, and 0.1% Triton X-100 (Sigma-Aldrich) to permeabilize the cells. Expression and localization of endogenously or ectopically expressed connexin was detected by labeling with a rabbit antibody against Cx43 (1:500, Sigma-Aldrich) or Cx30 (1:500, Invitrogen) for 1 hour. In some cases, cells were labeled with a mouse antibody against PDI (1:500, Enzo Life Sciences, Farmingdale, NY) to stain for the position of the ER, a mouse antibody against GM130 (1:500, BD Transduction Laboratories, Mississauga, Ontario, Canada) to demarcate the Golgi apparatus or a rabbit antibody against cleaved caspase-3 (1:1000, Cell Signaling Technology, Danvers, MA) to identify cells undergoing apoptosis. Cells were then incubated with secondary Alexa-Fluor-555- or Alexa-Fluor-488-conjugated antibodies (1:500, Invitrogen) for 45–60 minutes and stained for 5–10 minutes with Hoescht 33342 (1:1000, Invitrogen) to stain the nuclei. Cells were mounted on glass microscope slides. Cells that had been co-transfected with Cx30– or Cx26–RFP and GFP-tagged Cx30 mutants were not immunolabeled but were stained with Hoescht 33342 and mounted as described above. All slides were stored at 4℃ with minimal exposure to light. Slides were imaged by using a Zeiss LSM 510 confocal microscope (Carl Zeiss, Thornwood, NY) equipped with a 63× lens as previously outlined by Thomas and colleagues (Thomas et al., 2007).

Microinjection assays

In order to test wild-type Cx30 and mutant Cx30 gap junction function, REKs and HeLa cells that ectopically expressed the wild-type or mutants Cx30 proteins were microinjected with 10 mM Alexa-Fluor-350 hydrazide (Invitrogen) using an automated Eppendorf FemtoJet microinjection system (Eppendorf, Mississauga, Ontario, Canada) as previously described (Huang et al., 2013). For each biological replicate of

cells that expressed GFP, Cx30, T5M, V37E or G59R, ~15–20 cells were microinjected and the incidence of dye transfer to surrounding cells was recorded. Images were acquired by using a Leica DM IRE2 inverted epifluorescent microscope (Leica, Richmond Hill, Ontario, Canada) that was equipped with a Hamamatsu digital camera (Hamamatsu Photonics, Bridgewater, NJ) and OpenLab 5.5.3 imaging software (PerkinElmer, Lexington, MA). HeLa cells expressing the A88V mutant could not be microinjected because the cells were already undergoing cell death and had a permeable cell membrane; however, in the case of REKs, 5–10 cells were microinjected in each replicate. As positive and negative controls, REKs and HeLa cells were microinjected and processed in the same manner to ensure that cells were capable of GJIC and GJIC-deficient, respectively. A one-way ANOVA was performed on the means from three biological replicates, and the values represent the mean percent incidence of dye transfer±s.e.m.

Dye uptake hemichannel assays

To assess Cx30 and mutant hemichannel function, dye uptake assays were performed as previously described by Tong and colleagues (Tong et al., 2007) with some modifications. Briefly, HeLa cells that had been plated as single isolated cells were transfected with 1.5 µg of DNA as described above using Lipofectamine 2000. Normal ECS (142 mM NaCl, 5.4 mM KCl, 1.4 mM $MgCl_2$, 2 mM $CaCl_2$, 10 mM HEPES, 25 mM D-glucose, osmolarity 298 mOsm, pH adjusted to 7.35 by using NaOH) and DCF-ECS (as ECS except that Ca^{2+} and Mg^{2+} were replaced with 2 mM EGTA) were added to cells with 0.15 mM propidium iodide (molecular mass of 668.4 Da, Invitrogen). Groups of single isolated Cx30- or mutant-expressing cells were analyzed for their ability to take up propidium iodide under physiological (ECS) and Ca^{2+}- or Mg^{2+}-lacking (DCF-ECS) conditions. Images were taken under a 20× lens using the Leica microscope and OpenLab software. Isolated GFP-positive cells were quantified in the assay and ~60 cells were recorded for each biological replicate. The number of cells that exhibited dye uptake was recorded as a percentage of the total number of GFP-positive cells examined and a two-way ANOVA was performed on the means of four replicates. For determining cell integrity, a dextran–rhodamine-B (10 kDa, Invitrogen) uptake assay was performed. Briefly, Cx30–GFP and A88V–GFP-expressing cells were incubated in ECS containing 0.25% dextran–rhodamine-B. The number of cells that exhibited dye uptake was recorded as a percentage of the total number of GFP-positive cells and an unpaired Student's *t*-test was performed on the means of three independent experiments. Values represent the mean percentage of GFP-positive isolated cells that exhibited dye uptake±s.e.m.

TUNEL assays

TUNEL assays were performed using an ApopTag® Red *In Situ* Apoptosis Detection kit (EMD Millipore) as per the manufacturer's instructions with a few modifications. Briefly, control and mutant-expressing cells that had been grown in a monolayer were fixed in 10% NBF, permeabilized for 10 minutes with 0.5% Triton X-100 in PBS and subsequently washed with 1×PBS. Following the incubation period with the terminal deoxynucleotidyl transferase (TdT) enzyme at 37℃, cells were washed with working strength stop/wash buffer twice for 5 minutes per wash. Nuclei were stained with Hoescht 33342 and mounted. Images were obtained by using the Leica microscope and OpenLab Software with a 63× oil immersion objective lens. For each biological replicate of transfected cells and controls, 10–15 images were taken of random areas. The percentage of GFP-expressing cells that were positive for ApopTag labeling were calculated per image and a one-way ANOVA was performed on the means of three independent experiments. For controls, untransfected cells and those treated with staurosporin, the number of ApopTag-positive cells was recorded as a percentage of the total cell number. Values represent the mean percentage of apoptotic cells divided by the total number of cells per image±s.e.m.

XBP1 RT-PCR splicing assay

Processing of XBP1 mRNA, a marker of ER stress, was detected by PCR and restriction site analysis, as described elsewhere (Williams and Lipkin, 2006). Briefly, REKs were transfected with cDNA encoding wild-type Cx30 or the mutant proteins 12–24 hours before RNA extraction. As a positive control, untransfected cells were treated with the ER-stress-inducing compound tunicamycin (10 µg/ml) for 4–6 hours before RNA extraction. Total RNA was isolated from REKs and reverse-transcriptase (RT)-PCR was performed by using the RNeasy Mini and OneStep RT-PCR kits (Qiagen, Mississauga, Ontario, Canada), according to the manufacturer's instructions. Briefly, 1 µg of template RNA was reverse transcribed into cDNA in the first step of the RT-PCR cycle (50℃, 30 minutes) followed by amplification of the 601-bp XBP1 product, which encompasses the 26-bp intron sequence containing the *Pst*I restriction site, with the following primers: sense, 5′-AAACAGA-GTAGCAGCGCAGACTGC-3′; and antisense, 5′-GGATCTCTAAA-ACTAGAGGCTTGGTG-3′ for 35 cycles at 94℃ for 1 minute, 60℃ for 1 minute and 72℃ for 1 minute. To confirm expression of GFP-tagged wild-type or mutant Cx30 proteins, separate RT-PCR reactions with the following primers were performed to amplify a 315-bp eGFP product: sense, 5′-TCGTGACCACCCTGACCTAC-3′; and antisense, 5′-AGT-TCACCTTGATGCCGTTC-3′ for 35 cycles at 94℃ for 1 minute, 50℃ for 1 minute and 72℃ for 1 minute. Negative controls lacking the RNA template were included in every experiment. To determine whether the XBP1 products were spliced, half of the cDNA samples were incubated with *Pst*I restriction enzymes at 37℃ for 2 hours. All samples were resolved in 2% agarose gels and densitometry was performed on the bands using ImageJ (http://rsb.info.nih.gov/ij/).

Western blotting

Cell lysates were collected from cultures using a Triton-based extraction buffer [1% Triton X-100 (Sigma-Aldrich), 150 mM NaCl, 10 mM Tris, 1 mM EDTA, 1 mM ethylene glycol tetraacetic acid (EGTA), 0.5% nonyl phenoxypolyethoxylethanol (NP-40), 100 mM NaF, 100 mM sodium orthovanadate and proteinase inhibitor mini-EDTA tablet (Roche Applied Science, Laval, Quebec, Canada)] adjusted to pH 7.4 as previously described by Stewart and colleagues (Stewart et al., 2013). Extractions were repeated three times, and protein lysate concentrations were quantified by using a bicinchoninic acid (BCA) protein determination kit (Thermo Scientific, Rockford, IL). Total protein lysates of 50 µg were resolved by SDS-PAGE in 10% polyacrylamide gels and transferred to nitrocellulose membranes using the iBlot Dry Blotting System (Invitrogen). Membranes were then blocked using 5% Blotto Non-Fat Dry Milk (Santa Cruz Biotechnology) with 0.05% Tween-20 (Sigma-Aldrich) in PBS (PBS-T) for 30–60 minutes and subsequently incubated overnight at 4℃ with primary antibodies against Cx30 (1:750–1000, rabbit, Invitrogen), Cx43 (1:5000, rabbit, Sigma-Aldrich), GRP78 (1:500, goat, Santa Cruz Biotechnology), CHOP (3 µg/ml, mouse, Abcam, Toronto, Ontario, Canada) and ATF4 (5 µg/ml, mouse, Abcam). Gel loading controls included probing for the levels of β-tubulin using a primary mouse antibody against β-tubulin (1:10,000, Sigma-Aldrich). Blots that had been probed for Cx30 were counterstained with mouse antibodies against GFP (1:2500, EMD Millipore) to check that the GFP tag was attached to the wild-type and mutant Cx30 proteins. After several washes with PBS-T, blots were then incubated with secondary antibodies against rabbit or goat IgGs (conjugated to Alexa Fluor 680, 1:5000, Invitrogen) or against mouse IgGs (conjugated to IRdye 800, 1:5000, LI-COR Biosciences, Lincoln, NE) for 45–60 minutes. Following more PBS-T washes, blots were scanned and densitometry measurements were quantified by using the Odyssey Infrared Imaging System (LI-COR Biosciences). Each signal was normalized to its β-tubulin loading control in the same lane, and the outcome values of wild-type cells divided by that of β-tubulin, GFP divided by that of β-tubulin or Cx30 divided by that of β-tubulin was set to 1. Unpaired *t*-tests were performed on the fold-change means of these values from three distinct sets of protein lysates. Values represent the fold change±s.e.m.

Acknowledgements

We would like to thank Christian C. Naus for providing us with the pBluescript vector, as well as Vincent C. Hascall for providing us with the REKs used in this study. We would like to acknowledge Jessica Riley for her contributions to making the Cx30 mutant constructs.

Competing interests
The authors declare no competing interests.

Author contributions
A.C.B., J.J.K., C.S. and D.W.L. designed the experiments and interpreted this work. A.C.B. and J.J.K. performed the experiments, analyzed the data and wrote the manuscript. J.J.K. and D.W.L. revised the article. P.L. supplied DNA constructs and gave advice and assistance with the UPR experiments.

Funding
This study was supported by the Natural Sciences Engineering Research Council of Canada (a Canada Graduate Scholarship-Master's Program award to A.C.B.) and by the Canadian Institutes of Health Research (to D.W.L.).

Supplementary material
Supplementary material available online at
http://jcs.biologists.org/lookup/suppl/doi:10.1242/jcs.138230/-/DC1

References
Ahmad, S., Chen, S., Sun, J. and Lin, X. (2003). Connexins 26 and 30 are co-assembled to form gap junctions in the cochlea of mice. *Biochem. Biophys. Res. Commun.* **307**, 362-368.
Alapure, B. V., Stull, J. K., Firtina, Z. and Duncan, M. K. (2012). The unfolded protein response is activated in connexin 50 mutant mouse lenses. *Exp. Eye Res.* **102**, 28-37.
Alexander, D. B. and Goldberg, G. S. (2003). Transfer of biologically important molecules between cells through gap junction channels. *Curr. Med. Chem.* **10**, 2045-2058.
Anselmi, F., Hernandez, V. H., Crispino, G., Seydel, A., Ortolano, S., Roper, S. D., Kessaris, N., Richardson, W., Rickheit, G., Filippov, M. A. et al. (2008). ATP release through connexin hemichannels and gap junction transfer of second messengers propagate Ca2+ signals across the inner ear. *Proc. Natl. Acad. Sci. USA* **105**, 18770-18775.
Bakirtzis, G., Choudhry, R., Aasen, T., Shore, L., Brown, K., Bryson, S., Forrow, S., Tetley, L., Finbow, M., Greenhalgh, D. et al. (2003). Targeted epidermal expression of mutant Connexin 26(D66H) mimics true Vohwinkel syndrome and provides a model for the pathogenesis of dominant connexin disorders. *Hum. Mol. Genet.* **12**, 1737-1744.
Baris, H. N., Zlotogorski, A., Peretz-Amit, G., Doviner, V., Shohat, M., Reznik-Wolf, H. and Pras, E. (2008). A novel GJB6 missense mutation in hidrotic ectodermal dysplasia 2 (Clouston syndrome) broadens its genotypic basis. *Br. J. Dermatol.* **159**, 1373-1376.
Berridge, M. J. (2002). The endoplasmic reticulum: a multifunctional signaling organelle. *Cell Calcium* **32**, 235-249.
Beyer, E. C., Lin, X. and Veenstra, R. D. (2013). Interfering amino terminal peptides and functional implications for heteromeric gap junction formation. *Front Pharmacol* **4**, 67.
Bitner-Glindzicz, M. (2002). Hereditary deafness and phenotyping in humans. *Br. Med. Bull.* **63**, 73-94.
Boulay, A. C., del Castillo, F. J., Giraudet, F., Hamard, G., Giaume, C., Petit, C., Avan, P. and Cohen-Salmon, M. (2013). Hearing is normal without connexin30. *J. Neurosci.* **33**, 430-434.
Burra, S. and Jiang, J. X. (2011). Regulation of cellular function by connexin hemichannels. *Int. J. Biochem Mol. Biol.* **2**, 119-128.
Calfon, M., Zeng, H., Urano, F., Till, J. H., Hubbard, S. R., Harding, H. P., Clark, S. G. and Ron, D. (2002). IRE1 couples endoplasmic reticulum load to secretory capacity by processing the XBP-1 mRNA. *Nature* **415**, 92-96.
Chang, Q., Tang, W., Ahmad, S., Zhou, B. and Lin, X. (2008). Gap junction mediated intercellular metabolite transfer in the cochlea is compromised in connexin30 null mice. *PLoS ONE* **3**, e4088.
Chang, Q., Tang, W., Ahmad, S., Stong, B., Leu, G. and Lin, X. (2009). Functional studies reveal new mechanisms for deafness caused by connexin mutations. *Otol. Neurotol.* **30**, 237-240.
Chen, N., Xu, C., Han, B., Wang, Z. Y., Song, Y. L., Li, S., Zhang, R. L., Pan, C. M. and Zhang, L. (2010). G11R mutation in GJB6 gene causes hidrotic ectodermal dysplasia involving only hair and nails in a Chinese family. *J. Dermatol.* **37**, 559-561.
Choudhry, R., Pitts, J. D. and Hodgins, M. B. (1997). Changing patterns of gap junctional intercellular communication and connexin distribution in mouse epidermis and hair follicles during embryonic development. *Dev. Dyn.* **210**, 417-430.
Christianson, A. L. and Fourie, S. (1996). Family with autosomal dominant hidrotic ectodermal dysplasia: a previously unrecognised syndrome? *Am. J. Med. Genet.* **63**, 549-553.
Churko, J. M. and Laird, D. W. (2013). Gap junction remodeling in skin repair following wounding and disease. *Physiology (Bethesda)* **28**, 190-198.
Common, J. E., Becker, D., Di, W. L., Leigh, I. M., O'Toole, E. A. and Kelsell, D. P. (2002). Functional studies of human skin disease- and deafness-associated connexin 30 mutations. *Biochem. Biophys. Res. Commun.* **298**, 651-656.
Das Sarma, J., Wang, F. and Koval, M. (2002). Targeted gap junction protein constructs reveal connexin-specific differences in oligomerization. *J. Biol. Chem.* **277**, 20911-20918.
de Freitas, J. C. M., Jr, Silva, B. R., de Souza, W. F., de Araújo, W. M., Abdelhay, E. S. and Morgado-Díaz, J. A. (2011). Inhibition of N-linked glycosylation by tunicamycin induces E-cadherin-mediated cell-cell adhesion and inhibits cell proliferation in undifferentiated human colon cancer cells. *Cancer Chemother. Pharmacol.* **68**, 227-238.
De Vuyst, E., Decrock, E., De Bock, M., Yamasaki, H., Naus, C. C., Evans, W. H. and Leybaert, L. (2007). Connexin hemichannels and gap junction channels are differentially influenced by lipopolysaccharide and basic fibroblast growth factor. *Mol. Biol. Cell* **18**, 34-46.
Decrock, E., De Vuyst, E., Vinken, M., Van Moorhem, M., Vranckx, K., Wang, N., Van Laeken, L., De Bock, M., D'Herde, K., Lai, C. P. et al. (2009). Connexin 43 hemichannels contribute to the propagation of apoptotic cell death in a rat C6 glioma cell model. *Cell Death Differ.* **16**, 151-163.
Di, W. L., Rugg, E. L., Leigh, I. M. and Kelsell, D. P. (2001). Multiple epidermal connexins are expressed in different keratinocyte subpopulations including connexin 31. *J. Invest. Dermatol.* **117**, 958-964.
Di, W. L., Monypenny, J., Common, J. E., Kennedy, C. T., Holland, K. A., Leigh, I. M., Rugg, E. L., Zicha, D. and Kelsell, D. P. (2002). Defective trafficking and cell death is characteristic of skin disease-associated connexin 31 mutations. *Hum. Mol. Genet.* **11**, 2005-2014.
Essenfelder, G. M., Bruzzone, R., Lamartine, J., Charollais, A., Blanchet-Bardon, C., Barbe, M. T., Meda, P. and Waksman, G. (2004). Connexin30 mutations responsible for hidrotic ectodermal dysplasia cause abnormal hemichannel activity. *Hum. Mol. Genet.* **13**, 1703-1714.
Evans, W. H., Ahmad, S., Diez, J., George, C. H., Kendall, J. M. and Martin, P. E. (1999). Trafficking pathways leading to the formation of gap junctions. *Novartis Found. Symp.* **219**, 44-54, discussion 54-59.
Forge, A., Marziano, N. K., Casalotti, S. O., Becker, D. L. and Jagger, D. (2003). The inner ear contains heteromeric channels composed of cx26 and cx30 and deafness-related mutations in cx26 have a dominant negative effect on cx30. *Cell Commun. Adhes.* **10**, 341-346.
Fraser, F. C. and Der Kaloustian, V. M. (2001). A man, a syndrome, a gene: Clouston's hidrotic ectodermal dysplasia (HED). *Am. J. Med. Genet.* **100**, 164-168.
Galehdar, Z., Swan, P., Fuerth, B., Callaghan, S. M., Park, D. S. and Cregan, S. P. (2010). Neuronal apoptosis induced by endoplasmic reticulum stress is regulated by ATF4-CHOP-mediated induction of the Bcl-2 homology 3-only member PUMA. *J. Neurosci.* **30**, 16938-16948.
Gerido, D. A., DeRosa, A. M., Richard, G. and White, T. W. (2007). Aberrant hemichannel properties of Cx26 mutations causing skin disease and deafness. *Am. J. Physiol.* **293**, C337-C345.
Gong, X. Q., Shao, Q., Langlois, S., Bai, D. and Laird, D. W. (2007). Differential potency of dominant negative connexin43 mutants in oculodentodigital dysplasia. *J. Biol. Chem.* **282**, 19190-19202.
Gossman, D. G. and Zhao, H. B. (2008). Hemichannel-mediated inositol 1,4,5-trisphosphate (IP3) release in the cochlea: a novel mechanism of IP3 intercellular signaling. *Cell Commun. Adhes.* **15**, 305-315.
Grifa, A., Wagner, C. A., D'Ambrosio, L., Melchionda, S., Bernardi, F., Lopez-Bigas, N., Rabionet, R., Arbones, M., Monica, M. D., Estivill, X. et al. (1999). Mutations in GJB6 cause nonsyndromic autosomal dominant deafness at DFNA3 locus. *Nat. Genet.* **23**, 16-18.
Groenendyk, J. and Michalak, M. (2005). Endoplasmic reticulum quality control and apoptosis. *Acta Biochim. Pol.* **52**, 381-395.
Harris, A. L. (2007). Connexin channel permeability to cytoplasmic molecules. *Prog. Biophys. Mol. Biol.* **94**, 120-143.
He, L. Q., Liu, Y., Cai, F., Tan, Z. P., Pan, Q., Liang, D. S., Long, Z. G., Wu, L. Q., Huang, L. Q., Dai, H. P. et al. (2005). Intracellular distribution, assembly and effect of disease-associated connexin 31 mutants in HeLa cells. *Acta Biochim. Biophys. Sin. (Shanghai)* **37**, 547-554.
Hidvegi, T., Schmidt, B. Z., Hale, P. and Perlmutter, D. H. (2005). Accumulation of mutant alpha1-antitrypsin Z in the endoplasmic reticulum activates caspases-4 and -12, NFkappaB, and BAP31 but not the unfolded protein response. *J. Biol. Chem.* **280**, 39002-39015.
Hoang Dinh, E., Ahmad, S., Chang, Q., Tang, W., Stong, B. and Lin, X. (2009). Diverse deafness mechanisms of connexin mutations revealed by studies using in vitro approaches and mouse models. *Brain Res.* **1277**, 52-69.
Huang, T., Shao, Q., MacDonald, A., Xin, L., Lorentz, R., Bai, D. and Laird, D. W. (2013). Autosomal recessive GJA1 (Cx43) gene mutations cause oculodentodigital dysplasia by distinct mechanisms. *J. Cell Sci.* **126**, 2857-2866.
Jan, A. Y., Amin, S., Ratajczak, P., Richard, G. and Sybert, V. P. (2004). Genetic heterogeneity of KID syndrome: identification of a Cx30 gene (GJB6) mutation in a patient with KID syndrome and congenital atrichia. *J. Invest. Dermatol.* **122**, 1108-1113.
Jara, O., Acuña, R., García, I. E., Maripillán, J., Figueroa, V., Sáez, J. C., Araya-Secchi, R., Lagos, C. F., Pérez-Acle, T., Berthoud, V. M. et al. (2012). Critical role of the first transmembrane domain of Cx26 in regulating oligomerization and function. *Mol. Biol. Cell* **23**, 3299-3311.
Jordan, K., Solan, J. L., Dominguez, M., Sia, M., Hand, A., Lampe, P. D. and Laird, D. W. (1999). Trafficking, assembly, and function of a connexin43-green fluorescent protein chimera in live mammalian cells. *Mol. Biol. Cell* **10**, 2033-2050.
Kalvelyte, A., Imbrasaite, A., Bukauskiene, A., Verselis, V. K. and Bukauskas, F. F. (2003). Connexins and apoptotic transformation. *Biochem. Pharmacol.* **66**, 1661-1672.
Kibar, Z., Dubé, M. P., Powell, J., McCuaïg, C., Hayflick, S. J., Zonana, J., Hovnanian, A., Radhakrishna, U., Antonarakis, S. E., Benohanian, A. et al. (2000). Clouston hidrotic ectodermal dysplasia (HED): genetic homogeneity, presence of a founder effect in the French Canadian population and fine genetic mapping. *Eur. J. Hum. Genet.* **8**, 372-380.

Kikuchi, T., Adams, J. C., Miyabe, Y., So, E. and Kobayashi, T. (2000). Potassium ion recycling pathway via gap junction systems in the mammalian cochlea and its interruption in hereditary nonsyndromic deafness. *Med. Electron Microsc.* **33**, 51-56.
Kleizen, B. and Braakman, I. (2004). Protein folding and quality control in the endoplasmic reticulum. *Curr. Opin. Cell Biol.* **16**, 343-349.
Koval, M. (2006). Pathways and control of connexin oligomerization. *Trends Cell Biol.* **16**, 159-166.
Koval, M., Harley, J. E., Hick, E. and Steinberg, T. H. (1997). Connexin46 is retained as monomers in a trans-Golgi compartment of osteoblastic cells. *J. Cell Biol.* **137**, 847-857.
Kretz, M., Maass, K. and Willecke, K. (2004). Expression and function of connexins in the epidermis, analyzed with transgenic mouse mutants. *Eur. J. Cell Biol.* **83**, 647-654.
Kumar, N. M. and Gilula, N. B. (1996). The gap junction communication channel. *Cell* **84**, 381-388.
Kwon, T., Harris, A. L., Rossi, A. and Bargiello, T. A. (2011). Molecular dynamics simulations of the Cx26 hemichannel: evaluation of structural models with Brownian dynamics. *J. Gen. Physiol.* **138**, 475-493.
Lai, A., Le, D. N., Paznekas, W. A., Gifford, W. D., Jabs, E. W. and Charles, A. C. (2006). Oculodentodigital dysplasia connexin43 mutations result in non-functional connexin hemichannels and gap junctions in C6 glioma cells. *J. Cell Sci.* **119**, 532-541.
Laird, D. W. (2006). Life cycle of connexins in health and disease. *Biochem. J.* **394**, 527-543.
Laird, D. W., Jordan, K. and Shao, Q. (2001). Expression and imaging of connexin-GFP chimeras in live mammalian cells. *Methods Mol. Biol.* **154**, 135-142.
Lamartine, J., Munhoz Essenfelder, G., Kibar, Z., Lanneluc, I., Callouet, E., Laoudj, D., Lemaître, G., Hand, C., Hayflick, S. J., Zonana, J. et al. (2000). Mutations in GJB6 cause hidrotic ectodermal dysplasia. *Nat. Genet.* **26**, 142-144.
Langlois, S., Maher, A. C., Manias, J. L., Shao, Q., Kidder, G. M. and Laird, D. W. (2007). Connexin levels regulate keratinocyte differentiation in the epidermis. *J. Biol. Chem.* **282**, 30171-30180.
Lee, J. R., Derosa, A. M. and White, T. W. (2009). Connexin mutations causing skin disease and deafness increase hemichannel activity and cell death when expressed in Xenopus oocytes. *J. Invest. Dermatol.* **129**, 870-878.
Maeda, S., Nakagawa, S., Suga, M., Yamashita, E., Oshima, A., Fujiyoshi, Y. and Tsukihara, T. (2009). Structure of the connexin 26 gap junction channel at 3.5 A resolution. *Nature* **458**, 597-602.
Maher, A. C., Thomas, T., Riley, J. L., Veitch, G., Shao, Q. and Laird, D. W. (2005). Rat epidermal keratinocytes as an organotypic model for examining the role of Cx43 and Cx26 in skin differentiation. *Cell Commun. Adhes.* **12**, 219-230.
Malhotra, J. D. and Kaufman, R. J. (2007). The endoplasmic reticulum and the unfolded protein response. *Semin. Cell Dev. Biol.* **18**, 716-731.
Marziano, N. K., Casalotti, S. O., Portelli, A. E., Becker, D. L. and Forge, A. (2003). Mutations in the gene for connexin 26 (GJB2) that cause hearing loss have a dominant negative effect on connexin 30. *Hum. Mol. Genet.* **12**, 805-812.
McLachlan, E., Shao, Q. and Laird, D. W. (2007). Connexins and gap junctions in mammary gland development and breast cancer progression. *J. Membr. Biol.* **218**, 107-121.
Mese, G., Sellitto, C., Li, L., Wang, H. Z., Valiunas, V., Richard, G., Brink, P. R. and White, T. W. (2011). The Cx26-G45E mutation displays increased hemichannel activity in a mouse model of the lethal form of keratitis-ichthyosis-deafness syndrome. *Mol. Biol. Cell* **22**, 4776-4786.
Mhaske, P. V., Levit, N. A., Li, L., Wang, H. Z., Lee, J. R., Shuja, Z., Brink, P. R. and White, T. W. (2013). The human Cx26-D50A and Cx26-A88V mutations causing keratitis-ichthyosis-deafness syndrome display increased hemichannel activity. *Am. J. Physiol.* **304**, C1150-C1158.
Miwa, T., Minoda, R., Ise, M., Yamada, T. and Yumoto, E. (2013). Mouse otocyst transuterine gene transfer restores hearing in mice with connexin 30 deletion-associated hearing loss. *Mol. Ther.* **21**, 1142-1150.
Musil, L. S. and Goodenough, D. A. (1993). Multisubunit assembly of an integral plasma membrane channel protein, gap junction connexin43, occurs after exit from the ER. *Cell* **74**, 1065-1077.
Nemoto-Hasebe, I., Akiyama, M., Kudo, S., Ishiko, A., Tanaka, A., Arita, K. and Shimizu, H. (2009). Novel mutation p.Gly59Arg in GJB6 encoding connexin 30 underlies palmoplantar keratoderma with pseudoainhum, knuckle pads and hearing loss. *Br. J. Dermatol.* **161**, 452-455.
Nickel, R. and Forge, A. (2008). Gap junctions and connexins in the inner ear: their roles in homeostasis and deafness. *Curr. Opin. Otolaryngol. Head Neck Surg.* **16**, 452-457.
Pahl, H. L., Sester, M., Burgert, H. G. and Baeuerle, P. A. (1996). Activation of transcription factor NF-kappaB by the adenovirus E3/19K protein requires its ER retention. *J. Cell Biol.* **132**, 511-522.
Penuela, S., Bhalla, R., Gong, X. Q., Cowan, K. N., Celetti, S. J., Cowan, B. J., Bai, D., Shao, Q. and Laird, D. W. (2007). Pannexin 1 and pannexin 3 are glycoproteins that exhibit many distinct characteristics from the connexin family of gap junction proteins. *J. Cell Sci.* **120**, 3772-3783.
Rasheva, V. I. and Domingos, P. M. (2009). Cellular responses to endoplasmic reticulum stress and apoptosis. *Apoptosis* **14**, 996-1007.
Richard, G., Brown, N., Ishida-Yamamoto, A. and Krol, A. (2004). Expanding the phenotypic spectrum of Cx26 disorders: Bart-Pumphrey syndrome is caused by a novel missense mutation in GJB2. *J. Invest. Dermatol.* **123**, 856-863.
Ron, D. and Walter, P. (2007). Signal integration in the endoplasmic reticulum unfolded protein response. *Nat. Rev. Mol. Cell Biol.* **8**, 519-529.
Rouan, F., White, T. W., Brown, N., Taylor, A. M., Lucke, T. W., Paul, D. L., Munro, C. S., Uitto, J., Hodgins, M. B. and Richard, G. (2001). trans-dominant inhibition of connexin-43 by mutant connexin-26: implications for dominant connexin disorders affecting epidermal differentiation. *J. Cell Sci.* **114**, 2105-2113.
Saraste, A. and Pulkki, K. (2000). Morphologic and biochemical hallmarks of apoptosis. *Cardiovasc. Res.* **45**, 528-537.
Schütz, M., Scimemi, P., Majumder, P., De Siati, R. D., Crispino, G., Rodriguez, L., Bortolozzi, M., Santarelli, R., Seydel, A., Sonntag, S. et al. (2010). The human deafness-associated connexin 30 T5M mutation causes mild hearing loss and reduces biochemical coupling among cochlear non-sensory cells in knock-in mice. *Hum. Mol. Genet.* **19**, 4759-4773.
Smith, F. J., Morley, S. M. and McLean, W. H. (2002). A novel connexin 30 mutation in Clouston syndrome. *J. Invest. Dermatol.* **118**, 530-532.
Söhl, G. and Willecke, K. (2003). An update on connexin genes and their nomenclature in mouse and man. *Cell Commun. Adhes.* **10**, 173-180.
Söhl, G. and Willecke, K. (2004). Gap junctions and the connexin protein family. *Cardiovasc. Res.* **62**, 228-232.
Stewart, M. K., Gong, X. Q., Barr, K. J., Bai, D., Fishman, G. I. and Laird, D. W. (2013). The severity of mammary gland developmental defects is linked to the overall functional status of Cx43 as revealed by genetically modified mice. *Biochem. J.* **449**, 401-413.
Stong, B. C., Chang, Q., Ahmad, S. and Lin, X. (2006). A novel mechanism for connexin 26 mutation linked deafness: cell death caused by leaky gap junction hemichannels. *Laryngoscope* **116**, 2205-2210.
Stout, C. E., Costantin, J. L., Naus, C. C. and Charles, A. C. (2002). Intercellular calcium signaling in astrocytes via ATP release through connexin hemichannels. *J. Biol. Chem.* **277**, 10482-10488.
Subramanian, K. and Meyer, T. (1997). Calcium-induced restructuring of nuclear envelope and endoplasmic reticulum calcium stores. *Cell* **89**, 963-971.
Sugiura, K., Muro, Y., Futamura, K., Matsumoto, K., Hashimoto, N., Nishizawa, Y., Nagasaka, T., Saito, H., Tomita, Y. and Usukura, J. (2009). The unfolded protein response is activated in differentiating epidermal keratinocytes. *J. Invest. Dermatol.* **129**, 2126-2135.
Tang, Q., Dowd, T. L., Verselis, V. K. and Bargiello, T. A. (2009). Conformational changes in a pore-forming region underlie voltage-dependent ''loop gating'' of an unapposed connexin hemichannel. *J. Gen. Physiol.* **133**, 555-570.
Tattersall, D., Scott, C. A., Gray, C., Zicha, D. and Kelsell, D. P. (2009). EKV mutant connexin 31 associated cell death is mediated by ER stress. *Hum. Mol. Genet.* **18**, 4734-4745.
Teubner, B., Michel, V., Pesch, J., Lautermann, J., Cohen-Salmon, M., Söhl, G., Jahnke, K., Winterhager, E., Herberhold, C., Hardelin, J. P. et al. (2003). Connexin30 (Gjb6)-deficiency causes severe hearing impairment and lack of endocochlear potential. *Hum. Mol. Genet.* **12**, 13-21.
Thomas, T., Telford, D. and Laird, D. W. (2004). Functional domain mapping and selective trans-dominant effects exhibited by Cx26 disease-causing mutations. *J. Biol. Chem.* **279**, 19157-19168.
Thomas, T., Shao, Q. and Laird, D. W. (2007). Differentiation of organotypic epidermis in the presence of skin disease-linked dominant-negative Cx26 mutants and knockdown Cx26. *J. Membr. Biol.* **217**, 93-104.
Tong, D., Li, T. Y., Naus, K. E., Bai, D. and Kidder, G. M. (2007). In vivo analysis of undocked connexin43 gap junction hemichannels in ovarian granulosa cells. *J. Cell Sci.* **120**, 4016-4024.
Valiunas, V. and Weingart, R. (2000). Electrical properties of gap junction hemichannels identified in transfected HeLa cells. *Pflugers Arch.* **440**, 366-379.
Verselis, V. K. and Srinivas, M. (2008). Divalent cations regulate connexin hemichannels by modulating intrinsic voltage-dependent gating. *J. Gen. Physiol.* **132**, 315-327.
Verselis, V. K., Trelles, M. P., Rubinos, C., Bargiello, T. A. and Srinivas, M. (2009). Loop gating of connexin hemichannels involves movement of pore-lining residues in the first extracellular loop domain. *J. Biol. Chem.* **284**, 4484-4493.
Wang, W. H., Liu, Y. F., Su, C. C., Su, M. C., Li, S. Y. and Yang, J. J. (2011). A novel missense mutation in the connexin30 causes nonsyndromic hearing loss. *PLoS ONE* **6**, e21473.
Wangemann, P. (2006). Supporting sensory transduction: cochlear fluid homeostasis and the endocochlear potential. *J. Physiol.* **576**, 11-21.
Williams, B. L. and Lipkin, W. I. (2006). Endoplasmic reticulum stress and neurodegeneration in rats neonatally infected with borna disease virus. *J. Virol.* **80**, 8613-8626.
Yum, S. W., Zhang, J., Valiunas, V., Kanaporis, G., Brink, P. R., White, T. W. and Scherer, S. S. (2007). Human connexin26 and connexin30 form functional heteromeric and heterotypic channels. *Am. J. Physiol.* **293**, C1032-C1048.
Zhang, X. J., Chen, J. J., Yang, S., Cui, Y., Xiong, X. Y., He, P. P., Dong, P. L., Xu, S. J., Li, Y. B., Zhou, Q. et al. (2003). A mutation in the connexin 30 gene in Chinese Han patients with hidrotic ectodermal dysplasia. *J. Dermatol. Sci.* **32**, 11-17.
Zhang, Y., Tang, W., Ahmad, S., Sipp, J. A., Chen, P. and Lin, X. (2005). Gap junction-mediated intercellular biochemical coupling in cochlear supporting cells is required for normal cochlear functions. *Proc. Natl. Acad. Sci. USA* **102**, 15201-15206.
Zhao, H. B., Yu, N. and Fleming, C. R. (2005). Gap junctional hemichannel-mediated ATP release and hearing controls in the inner ear. *Proc. Natl. Acad. Sci. USA* **102**, 18724-18729.
Zhao, H. B., Kikuchi, T., Ngezahayo, A. and White, T. W. (2006). Gap junctions and cochlear homeostasis. *J. Membr. Biol.* **209**, 177-186.

Journal of Cell Science

Fig. S1. Expression of the V37E and A88V mutants reduced the incidents of co-expressed Cx43 being found in gap junctions. HeLa cells were engineered to co-express GFP-tagged Cx30 and T5M, V37E, G59R and A88V mutants (green) with Cx43-RFP (red). Cx30 and T5M showed co-localization in gap junction-like plaques with Cx43. The V37E and A88V mutants showed intracellular accumulations that co-localized with Cx43 and reduced Cx43 plaques were evident. The G59R mutant localized intracellularly, but it did not appear to affect the ability of Cx43 to reach the cell surface. Scale bar=20 ∀m.

Fig. S2. REKs expressing V37E and A88V mutants express cleaved caspase-3. Untransfected (Untr) cells or GFP-, Cx30- and mutant-expressing REKs (green) were immunolabeled for cleaved caspase-3 (red) and nuclei were stained with Hoescht 33342 (blue). Cells expressing the V37E and A88V mutants also expressed the apoptotic marker cleaved caspase-3. Scale bar=20 ∀m.

Fig. S3. Western blot analysis of the unfolded protein response in mutant-expressing REKs. The levels of unfolded protein response (UPR) markers glucose regulated protein 78 (GRP78) (A), activating transcription factor 4 (ATF4) (B) and C/EBP homologous protein (CHOP) (C) in untransfected (Untr) and GFP-, Cx30- and mutant-expressing REKs were analyzed and normalized to β-tubulin. Protein lysates from tunicamycin (Tm)-treated cells served as an inducer of the UPR. Blots were also probed with anti-β-tubulin antibody. Normalized values for Untr cells were set to 1. (**A**) In comparison to GFP-expressing cells, GRP78 expression was significantly higher in Tm-treated controls (***P<0.001) and not in cells expressing the mutants. (**B**) In comparison to GFP-expressing cells, ATF4 expression was higher in V37E-expressing cells (*P<0.05) and Tm-treated controls only (**P<0.01). (**C**) CHOP was also only upregulated in Tm-treated cells only (*P<0.05 and **P<0.01). Values represent fold change ± s.e.m. (unpaired Student's *t*-test, N=3). **(D, E)** Upon activation, IRE1 cleaves an intron (black box) from XBP1 mRNA to yield a spliced variant without a *Pst*I site. The possible band sizes produced by splicing and *Pst*I digestion are shown in the table. (**F**) RNA from untransfected REKs (Untr), REKs treated with tunicamycin (Tm) and REKs expressing Cx30 or Cx30 mutants was analyzed by RT-PCR using primers that amplified both the spliced (XBP1s) and unspliced (XBP1u) variants. Upper panel shows a representative gel separation of undigested and *Pst*1 digested bands. Note the loss of XBP1u bands (289 bp and 312 bp) and increased intensity of the XBP1s band (575 bp) for the Tm control. All other band intensities were similar between Untr and Cx30 mutants. The lower panel represents a higher resolution image of the *Pst*I undigested bands showing the separation of XBP1u and XBP1s. (**G**) Densitometry quantification and ratio of upper (575–601 bp) to lower (289–312 bp) bands showed no significant increase in XBP1 splicing for any of the mutants, whereas the Tm control significantly induced a ~3.5 fold increase in XBP1s. Values represent fold change ± s.e.m. (one way ANOVA, ***P<0.001, N=6).

Fig. S4. Cx30 and Cx26 may partially rescue the trafficking of V37E and A88V mutants in HeLa cells. HeLa cells co-expressing Cx30-RFP (red) together with GFP-tagged Cx30, T5M, V37E, G59R or A88V mutants (green) were stained with Hoescht 33342 (blue) to denote the cell nuclei. Cx30, T5M and populations of the V37E, G59R and A88V mutants distinctly co-localized with Cx30-RFP at the cell surface, however all skin disease-linked mutants were primarily intracellularly localized. HeLa cells co-expressing Cx26-RFP (red) and GFP-tagged Cx30, T5M, V37E, G59R or A88V mutants (green) were stained with Hoescht 33342 (blue) to denote the nuclei. Cx30 and T5M co-localized strongly with Cx26-RFP at the cell surface, as did the G59R mutant. There were marked reductions in Cx26-RFP gap junction plaques in both V37E and A88V expressing cells and an increase in intracellular Cx26-RFP co-localization. Scale Bars=20 ∀m.

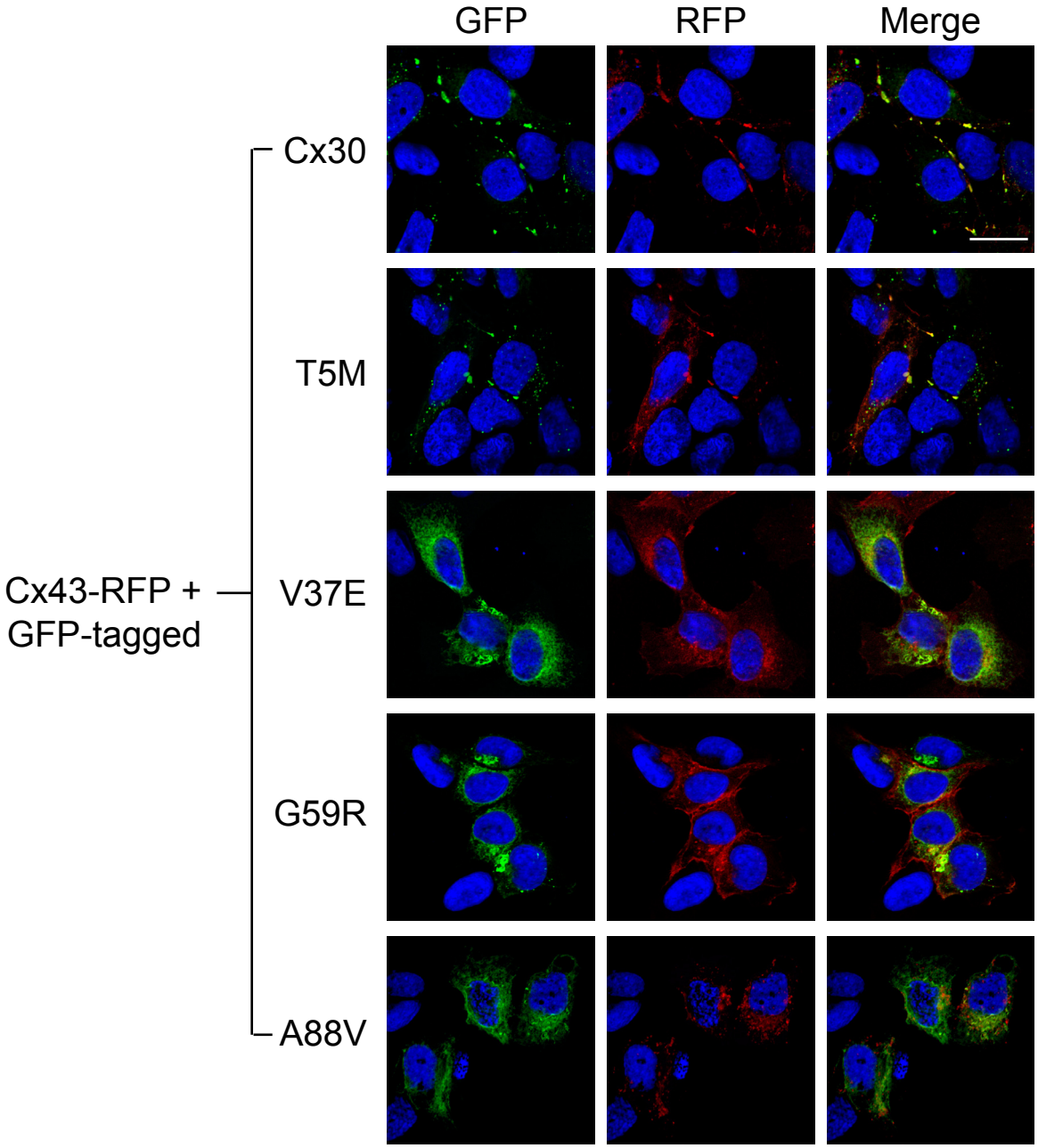

FIGURE S1

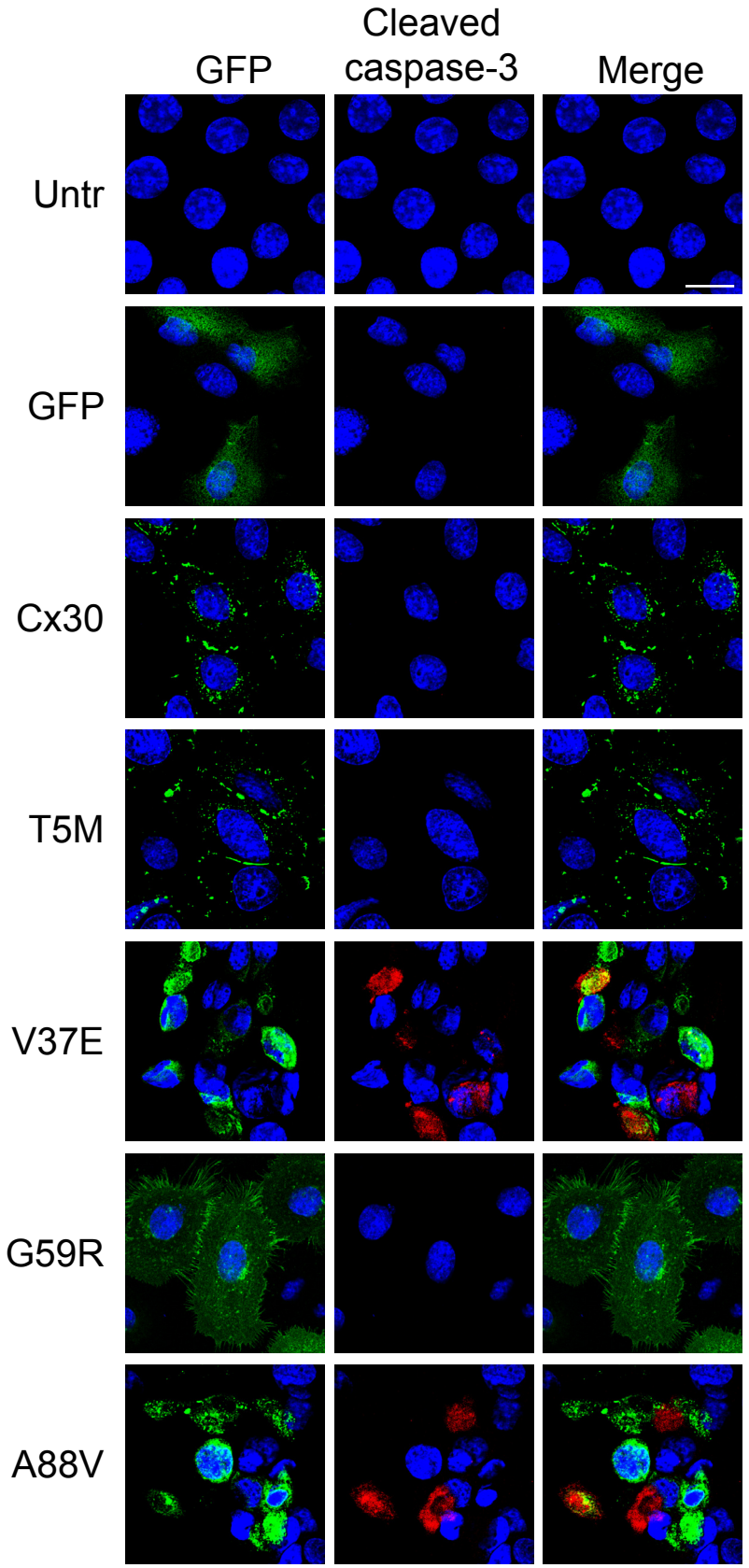

FIGURE S2

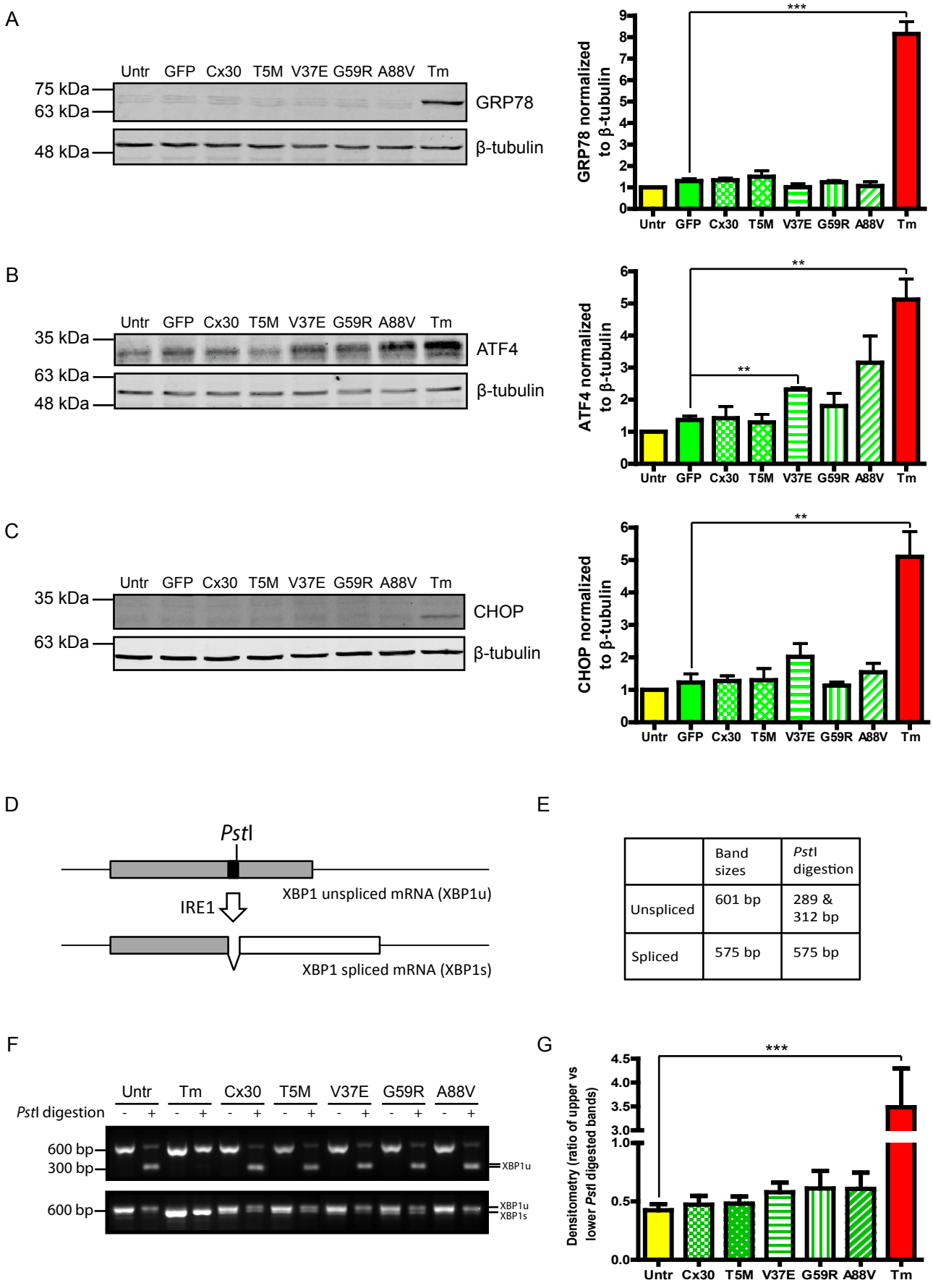

	Band sizes	*Pst*I digestion
Unspliced	601 bp	289 & 312 bp
Spliced	575 bp	575 bp

FIGURE S3

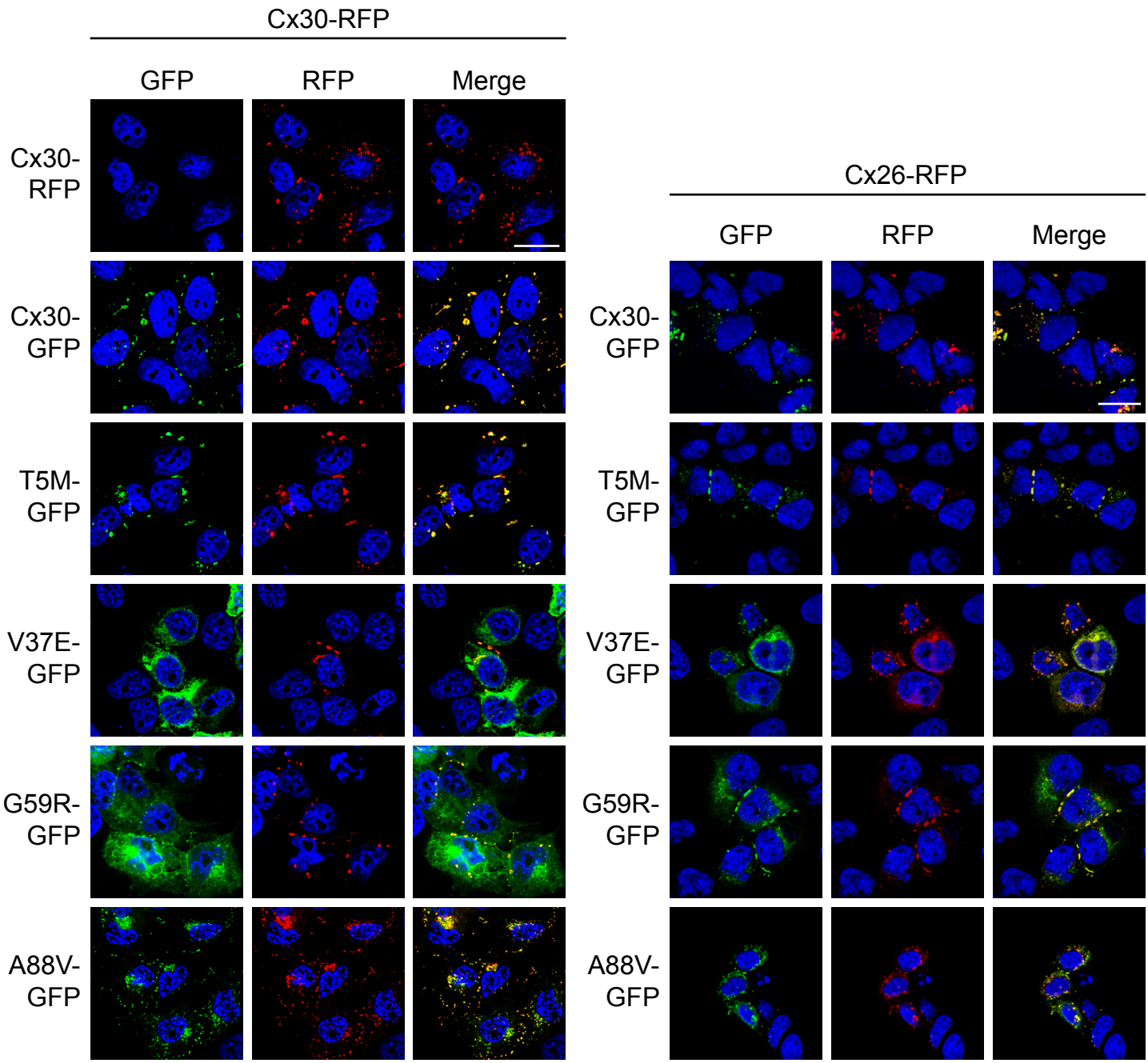
Cx30-RFP
GFP
RFP
Merge
Cx30-RFP
Cx30-GFP
T5M-GFP
V37E-GFP
G59R-GFP
A88V-GFP
Cx26-RFP
GFP
RFP
Merge
Cx30-GFP
T5M-GFP
V37E-GFP
G59R-GFP
A88V-GFP

FIGURE S4